

Source-Resolved Variability of Fine Particulate Matter and Human Exposure in an Urban Area

Pablo Garcia Rivera¹, Brian T. Dinkelacker¹, Ioannis Kioutsioukis²,
Peter J. Adams^{3,4}, and Spyros N. Pandis^{5,6}

¹Department of Chemical Engineering, Carnegie Mellon University, Pittsburgh, PA, 15213

²Department of Physics, University of Patras, 26500, Patras, Greece

³Department of Civil and Environmental Engineering, Carnegie Mellon University, Pittsburgh, PA, 15213

⁴Department of Engineering and Public Policy, Carnegie Mellon University, Pittsburgh, PA, 15213

⁵Institute of Chemical Engineering Sciences (FORTH/ICE-HT), 26504, Patras, Greece

⁶Department of Chemical Engineering, University of Patras, 26500, Patras, Greece

Abstract

Increasing the resolution of chemical transport model (CTM) predictions in urban areas is important to capture sharp spatial gradients in atmospheric pollutant concentrations and better inform air quality and emissions controls policies that protect public health. The chemical transport model PMCAMx was used to assess the impact of increasing model resolution on the ability to predict the source-resolved variability and population exposure to PM_{2.5} at 36 x 36, 12 x 12, 4 x 4, and 1 x 1 km resolutions over the city of Pittsburgh during typical winter and summer periods (February and July 2017). At the coarse resolution, county-level differences can be observed, while increasing the resolution to 12 x 12 km resolves the urban-rural gradient. Increasing resolution to 4 x 4 km resolves large stationary sources such as power plants and the 1 x 1 km resolution reveals intra-urban variations and individual roadways within the simulation domain. Regional pollutants that exhibit low spatial variability such as PM_{2.5} nitrate show modest changes when increasing the resolution beyond 12 x 12 km. Predominantly local pollutants such as elemental carbon

and [primary](#) organic aerosol have gradients that can only be resolved at the 1 x 1 km scale. Contributions from some local sources are enhanced by weighting the average contribution from each source by the population in each grid cell. The average population weighted PM_{2.5} concentration does not change significantly with resolution, suggesting that extremely high resolution PM_{2.5} predictions may not be necessary for effective urban epidemiological analysis.

1. Introduction

Particulate matter with aerodynamic diameter less than 2.5 µm (PM_{2.5}) contributes to poor air quality throughout large parts of the United States. These particles directly affect visibility (Seinfeld and Pandis, 2006) and have been associated with long and short-term health effects such as premature death due to cardiovascular disease, increased chance of heart attacks and strokes, [and](#) reduced lung development and function in children and people with lung diseases such as asthma ~~and increases in hospital admissions due to heart and lung disease~~ (Dockery and Pope, 1994).

At high resolutions, emissions from local sources such as commercial cooking, on-road traffic, residential wood combustion, and industrial activities can have sharp gradients that influence the geographical distribution of PM_{2.5} concentrations. High-resolution measurements of PM₁ have found gradients of up to ~2 µg m⁻³ between urban background sites and those with high local emissions (Gu et al., 2018; Robinson et al., 2018).

A key limiting factor on the modeling of particulate matter at high resolutions is the geographical distribution of emissions. Previous studies have found that coarse grid emissions interpolated to higher resolutions lead to small to modest improvements in model predictive ability for ozone (Arunachalam et al., 2006; Kumar and Russell, 1996), secondary organic aerosol (Fountoukis et al., 2013; Stroud et al., 2011) and nitrate (Zakoura and Pandis, 2019, 2018). Pan et al., (2017) used the default approach from the U.S. Environmental Protection Agency (EPA) National Emissions Inventory (NEI) to allocate county-based emissions to model grid cells at 4 x 4 and 1 x 1 km and found only small changes to model performance for NO_x and O₃, while the 1 x 1 km case showed more detailed features of emissions and concentrations in heavily polluted areas.

Improvements in the resolution of emission inventories have been focused on traffic as this source exhibits significant variability at high resolutions. Recent approaches to building high-resolution traffic inventories include origin-destination by vehicle class (Ma et al., 2020), synthetic population mobility (Elessa Etuman and Coll, 2018) and fuel sales combined with traffic counts (McDonald and McBride, 2014). Other sectors such as biomass burning for residential heating and commercial cooking have been identified as very uncertain in current inventories (Day et al., 2019). Recent versions of the NEI have made progress addressing the total emissions and temporal distributions of biomass burning and commercial cooking (Eyth and Vukovich, 2016), but there is still significant uncertainty on their geographical location at a sub-county scale. Robinson et al. (2018) found greatly elevated organic aerosol concentrations (10s of $\mu\text{g m}^{-3}$) in the vicinity of numerous individual restaurants and commercial districts containing groups of restaurants indicating that commercial cooking is a source of large gradients on the urban scale.

Population density and socio-economic indicators of that population, such as income or access to healthcare, show large gradients in the urban scale. It is important to assess the exposure of different sub-populations to air pollutants and the resulting health effects, a concept known as Environmental Justice (Anand, 2002).

We use the Particulate Matter Comprehensive Air quality Model with Extensions (PMCAMx) to study the impact of increasing model resolution on the model's ability to predict the variability, sources and population exposure of $\text{PM}_{2.5}$ concentrations on the urban scale in Pittsburgh. We compare predicted variability at 36 x 36, 12 x 12, 4 x 4 and 1 x 1 km resolutions over the city of Pittsburgh during one typical summer and one typical winter month of 2017. Additional sensitivity simulations were performed to determine contributions from selected sources to concentrations. The results of the simulations are used to estimate exposure to $\text{PM}_{2.5}$ at all resolutions and from the selected sources. A detailed evaluation of the PMCAMx predictions against measurements will be the topic of a future publication. Overall the model performance was similar to those in previous model applications in the Eastern US (Fountoukis et al., 2013).

2. PMCAMx Description

The Particulate Matter Comprehensive Air quality Model with Extensions (PMCAMx) (Karydis et al., 2010; Murphy and Pandis, 2004; Tsimpidi et al., 2010), uses the framework of the CAMx model (Environ, 2006) to describe horizontal and vertical advection and diffusion, emissions, wet and dry deposition, gas, aqueous and aerosol-phase chemistry. A 10-size section aerosol sectional approach is used to dynamically track the evolution of the aerosol mass distribution. The aerosol species modeled include sulfate, nitrate, ammonium, sodium, chloride, elemental carbon, water, primary and secondary organics, and other non-volatile aerosol components. The SAPRC (Statewide Air Pollution Research Center) photochemical mechanism (Carter, 1999) is used for the simulation of gas-phase chemistry. The version of SAPRC used here includes 237 reactions and 91 individual and surrogate species. For inorganic growth, a bulk equilibrium approach was used, assuming equilibrium between the bulk inorganic aerosol and gas phases (Pandis et al., 1993). [Aqueous-phase chemistry is simulated using the Variable Size Resolution Model \(VSRM\) \(Fahey and Pandis, 2001\).](#) The partitioning of the various semivolatile inorganic aerosol components and aerosol water is determined using the ISORROPIA-I aerosol thermodynamics model (Nenes et al., 1998). The primary and secondary organic aerosol components are described using the volatility basis set approach (Donahue et al., 2006). For primary organic aerosol (POA) ten volatility bins, with effective saturation concentrations ranging from 10^{-3} to $10^6 \mu\text{g m}^{-3}$ at 298 K are used. [The volatility distribution for POA from Tsimpidi et al. \(2010\) was used for all sources, while size distributions are specific to each emission sector.](#) Anthropogenic (aSOA) and biogenic (baSOA) are modeled with 4 volatility bins ($1, 10, 10^2, 10^3 \mu\text{g m}^{-3}$) (Murphy and Pandis, 2009) using NO_x dependent yields (Lane et al., 2008). [Both fine and coarse mode PM are modeled simulated by in this formulation of PMCAMx, although the following analyses in this work are-is focused on fine PM_{2.5}-mass.](#) More detailed descriptions of PMCAMx can be found in Fountoukis et al. (2011) and Zakoura and Pandis (2018).

3. Model Application

PMCAMx was used to simulate air quality over the metropolitan area of Pittsburgh during February and July 2017. For the base-case simulation we used a one-way nested

structure with a 36 x 36 km master grid covering the continental United States, with nested grids of 12 x 12 km, 4 x 4 km in South Western Pennsylvania and a 1 x 1 km grid covering the city of Pittsburgh, most of Allegheny County and the upper Ohio River valley (Figure 1a). The 1 x 1 km grid covers a 72 x 72 km area (Figure 1b). Two days in each simulation were used for model spin-up and discarded for all analyses. –Simulations required approximately 6 CPU days, 5 CPU hours, 10 CPU hours, and 12 CPU days to complete in a single Intel Xeon CPU E5-4640 at 2.4 GHz for the 36 km, 12 km, 4 km, and 1 km domains, respectively.

The surface concentrations at the boundaries of the 36 x 36 km grid are shown in **Error! Reference source not found.** in the Supplementary Information. These values were applied to all upper air layers assuming a constant mixing ratio. Results from lower resolution simulations were used as boundary conditions for the corresponding next higher resolution simulation. Horizontal wind components, vertical diffusivity, temperature, pressure, water vapor, clouds, and rainfall were generated using the Weather Research and Forecasting (WRF v3.6.1) model over the whole modeling domain with horizontal resolution of 12 km. The data was interpolated to higher resolutions when needed. –The interpolation of meteorological fields from 12 x 12 km to higher resolutions is a potential limitation of this work and will be the focus of future improvements to the modeling methods,; although it is likely that the use of 1 x 1 km resolution meteorological fields would present difficulties in the modeling of plume dispersion in the narrow valleys present in the inner domain. Initial and boundary meteorological conditions for the WRF simulations were generated from the ERA-Interim global climate re-analysis database, together with the terrestrial data sets for terrain height, land-use, soil categories, etc. from the United States Geological Survey (USGS) database. The WRF modeling system was prepared and configured in a similar way as described by Gilliam and Pleim (2010). This configuration is recommended for air quality simulations (Hogrefe et al., 2015; Rogers et al., 2013). 28 vertical layers were used in the WRF simulations modeling to produce 14 layers of meteorological input for the PMCAMx simulations. Each of the 14 PMCAMx layers corresponds to a WRF layer.

Emissions were calculated using the EPA’s Emission Modeling Platform (v6.3) for the National Emissions Inventory for 2011 (NEI11) (Eyth and Vukovich, 2016) using the

default 2017 projected values. Base emissions were calculated first at a 12 km resolution for the full modeling domain using the Sparse Matrix Operator Kernel Emissions (SMOKE) model and our WRF meteorological data. [The data sources used to produce 12 km resolution surrogates with Platform v6.3 were used to develop surrogates at 4 x 4 km and 1 x 1 km resolution](#) ~~For the higher resolution grids, the spatial surrogates provided with Platform v6.3 were used~~ for all sectors except commercial cooking and on-road traffic for which custom surrogates were developed. [These custom surrogates also use projected values for 2017. Bicubic interpolation was used to produce biogenic emissions at 4 x 4 km and 1 x 1 km resolution, wherein areas in which sufficient data was unavailable.](#) The emissions by all sources together with the chemical composition are summarized in Tables 1 (for the winter period) and 2 (for the summer period)..

In this work, we used normalized restaurant count to distribute the commercial cooking emissions in space in the 1x1 km [and 4x4 km resolution](#) ~~inner~~ domains. Geographical information was collected for all locations labeled as “restaurant” from the freely accessible Google Places Application Programming Interface (API) for the western Pennsylvania area, eastern Ohio and northern West Virginia. Using this new spatial surrogate, PM_{2.5} emissions from commercial cooking are enhanced primarily in the Pittsburgh urban core with a maximum increase of 1200 kg ~~dg~~⁻¹ km⁻² (Figure 2a).

To accurately capture spatial patterns of on-road traffic, we use the output of a link-level, origin-destination by vehicle class traffic model of Pittsburgh (Ma et al., 2020). This traffic model simulates traffic counts and speed by hour-of-day using observations from Pennsylvania Department of Transportation sites throughout Pittsburgh. As expected, emissions in areas with major highways are high (Figure 2b).

[The novel surrogates used for onroad traffic and cooking result in ~~small~~ increases in predicted PM_{2.5} concentration emissions in some areas and, particularly in downtown the urban area of Pittsburgh and decreases in others. Total emissions inside the inner 1 x 1 km domain are the same using both the new and old surrogates. For commercial cooking, emissions calculated using the new surrogates are more concentrated in areas with high restaurant densities such as downtown Pittsburgh and the Oakland neighborhood \(Figures S1 and S2\). For onroad traffic, the emissions become higher at the locations of major highways and in the urban area of Pittsburgh when using the new surrogates \(Figures S3](#)

and S4). Using the new spatial distribution of emissionsThe predicted average $PM_{2.5}$ increase by ~~largest difference seen was an increase in~~ $1-2 \mu g m^{-3}$ ~~on average at certain areas. the locations of low-cost sensors (RAMPs) in the urban area of Pittsburgh. A detailed evaluation of these predictions will be the topic of another publication. A summary of prediction performance using the new surrogates is provided in Table S2 of the supplementary material and a more detailed evaluation will be included in a following publication.~~

4. $PM_{2.5}$ concentrations and sources during winter

4.1 Effect of grid resolution

The results of the simulations with the four resolutions for the winter period are shown in Figures **Error! Reference source not found.** and **Error! Reference source not found.**. For the area of interest, the simulations at 36 x 36 km resolves concentration fields at the county scale. The urban-rural gradient is resolved in the 12 x 12 km simulations. Increasing the resolution to 4 x 4 km, large stationary sources such as power plants and large industrial installations are resolved. Finally, the resolution increase to 1 x 1 km resolves the intra-urban variations in Pittsburgh and medium-sized industrial installations.

[Variable concentration limits are used in the species maps to remove background and highlight the effects of local sources \(Figures 3 and 4\).](#)

In the winter period, the predicted maximum $PM_{2.5}$ concentration in the inner domain increases from $10.4 \mu g m^{-3}$ at 36x36 km, to $11.8 \mu g m^{-3}$ at 12x12, to $12.9 \mu g m^{-3}$ at 4x4, and finally to $16.4 \mu g m^{-3}$ at 1x1 km (Figure 3), a 58% increase. On the other end, the predicted minimum $PM_{2.5}$ concentration changes from $8.2 \mu g m^{-3}$ at 36 x 36 km to $7 \mu g m^{-3}$ at 12 x 12 and remains practically the same at even higher resolutions. This corresponds to the “background” concentration level for the area during the simulation period, so further resolution enhancements do not change this value. The standard deviation of the predicted concentration can be used as a measure of the concentration variability in the area. This standard deviation changes from $0.9 \mu g m^{-3}$ at 36x36, to $1.24 \mu g m^{-3}$ at 12x12, to $1.45 \mu g m^{-3}$ at 4x4 and to $1.35 \mu g m^{-3}$ at 1x1 km. These results indicate an increase of the $PM_{2.5}$ variability by 50% when one moves from the coarse to the finest resolution. However, most

of this change in variability (38% out of the 50%) appears when one moves from 36x36 to 12x12 km.

Elemental carbon is a primary aerosol component with sources that are quite variable in space. In winter, the predicted maximum $\text{PM}_{2.5}$ EC increased by a factor of 2.9, from $0.6 \mu\text{g m}^{-3}$ at the 36 x 36 km resolution to $1.6 \mu\text{g m}^{-3}$ at 1 x 1 km (Figure 3). The predicted maximum EC is, as expected in the Pittsburgh downtown area. On the other hand, the predicted minimum of EC is reduced by only $0.1 \mu\text{g m}^{-3}$, from $0.34 \mu\text{g m}^{-3}$ at 36x36 km to $0.24 \mu\text{g m}^{-3}$ at resolutions lower or equal than 4x4 km. The standard deviation of the predicted EC almost doubles from $0.1 \mu\text{g m}^{-3}$ at 36 x 36 km to $0.18 \mu\text{g m}^{-3}$ at 1 x 1 km. Approximately 50% of this increase in variability appears in the transition from the coarse to the intermediate resolution of 12 x 12 km. The fine and the finest resolutions are needed to resolve the other half of the predicted variability.

During this winter period a significant fraction (79%) of the OA in the Pittsburgh area is primary and therefore the higher resolution results in increases of the predicted maximum concentrations in space from $2.8 \mu\text{g m}^{-3}$ at the coarse resolution to $3.7 \mu\text{g m}^{-3}$ at the intermediate to $4.8 \mu\text{g m}^{-3}$ at the finest resolution (Figure 3). This corresponds to an increase by a factor of 1.7, more than the change for total $\text{PM}_{2.5}$, but much less than that for EC. The predicted maximum is located in downtown Pittsburgh, with additional hotspots in neighboring counties that are resolved at the fine and finest resolution. The predicted minimum changes from $2.1 \mu\text{g m}^{-3}$ at 36x36 to $1.7 \mu\text{g m}^{-3}$ at 12x12 with small reductions at higher resolutions. The variability (standard deviation) of the OA concentration field of the predicted concentration increases by a factor of approximately 1.6 from $0.35 \mu\text{g m}^{-3}$ at 36 x 36, to $0.51 \mu\text{g m}^{-3}$ at 12 x 12 km. The increase is small at even higher resolutions with the standard deviation of OA reaching $0.53 \mu\text{g m}^{-3}$ at 1 x 1 km (an increase by a factor of 1.7).

Average predicted $\text{PM}_{2.5}$ sulfate in the inner domain changes little between the coarsest resolution (average level $1.37 \mu\text{g m}^{-3}$) and finest resolution ($1.29 \mu\text{g m}^{-3}$). The minimum concentration decreased slightly with resolution from 1.33 to $1.2 \mu\text{g m}^{-3}$, with much of the decrease captured by increasing the resolution to 12 x 12 km (~~$1.33 \mu\text{g m}^{-3}$ at 36 x 36 km and $1.20 \mu\text{g m}^{-3}$ at 12 x 12 km~~). The maximum sulfate concentration increased by a larger value but this change was not observed until moving to the highest resolution

where the maximum was $2.08 \mu\text{g m}^{-3}$, compared to $1.40 \mu\text{g m}^{-3}$ at $36 \times 36 \text{ km}$ resolution. The standard deviation increased only marginally from $0.03 \mu\text{g m}^{-3}$ at $36 \times 36 \text{ km}$ to $0.06 \mu\text{g m}^{-3}$ at $1 \times 1 \text{ km}$. The low variability in the predicted ground sulfate levels during the winter is partially due ~~Much of the increase in local variability of sulfate seen in the summer is not seen here due to the lower mixing heights during this cold period -in winter paired with the emissions from the tall emissions-~~ stacks of local power generation sources often introduced above the boundary layer. ~~which contribute a majority of the local sulfate emissions (Table 1).~~

The predicted fine nitrate levels are relatively high ranging from 1.78 to $2.24 \mu\text{g m}^{-3}$ in the coarse-resolution simulation. This is expected in this wintertime period due to the partitioning of nitric acid and ammonium in the particulate phase. This predicted concentration range increases to 1.5 - $2.24 \mu\text{g m}^{-3}$ in the finest scale simulation with higher levels in the northeast of the domain. The standard deviation of the predicted concentration does not show any significant trend changing from $0.19 \mu\text{g m}^{-3}$ at 36×36 to $0.15 \mu\text{g m}^{-3}$ at $1 \times 1 \text{ km}$.

For $\text{PM}_{2.5}$ ammonium, changes with increasing resolution are modest with the predicted minimum being reduced from $1.07 \mu\text{g m}^{-3}$ at 36×36 to approximately $0.95 \mu\text{g m}^{-3}$ at all other higher resolutions. The predicted maximum stays relatively constant between $1.25 \mu\text{g m}^{-3}$ and $1.27 \mu\text{g m}^{-3}$ at all resolutions. As with nitrate, the standard deviation does not show any significant trend changing from $0.08 \mu\text{g m}^{-3}$ at 36×36 , to $0.09 \mu\text{g m}^{-3}$ at 12×12 , to $0.07 \mu\text{g m}^{-3}$ at 4×4 and $1 \times 1 \text{ km}$ resolutions.

4.2 Source Apportionment

We performed zero-out simulations in the $1 \times 1 \text{ km}$ Pittsburgh grid to determine the local contributions of eight source categories to the total $\text{PM}_{2.5}$. The local sources quantified included: commercial cooking, industrial, biomass burning, on-road traffic, power generation, and miscellaneous area sources. A summary of total local (within the inner $1 \times 1 \text{ km}$ resolution domain) dry $\text{PM}_{2.5}$ emissions from each source category during February 2017 is shown in Table 1. The species category labeled “other” for the power generation sector is predominately composed of ash (including metals emitted from power generation) and is simulated in PMCAMx as inert particle mass. -Biomass burning

emissions here correspond only to residential wood combustion, as there were no significant wildfires in the 1 x 1 km resolution domain during the simulation periods. The PM_{2.5} emissions used in this study contain both the condensable and filterable fractions of PM_{2.5} (U.S. EPA, 2015). The miscellaneous area sources sector includes a large variety of emission sources that are not classified in any of the sources in ~~Table 2~~Table 1. These include chemical manufacturing, solvent utilization for surface coatings, degreasing and dry cleaning, storage and transport of petroleum products, waste disposal and incineration, and cremation. The emissions from agricultural dust, river barges, off-road equipment, oil-gas activities, and rail were grouped on the “others” source. All emissions (particulate and gas-phase) from each source were set to zero, and the results of the zero-out simulation were subtracted from those of the baseline simulation to estimate the corresponding source contribution. The contribution of long-range transport from outside the inner domain was also estimated by setting all local sources to zero.

Biomass burning is used during the winter for residential heating and recreation. This source contributes a maximum of 3.31 $\mu\text{g m}^{-3}$ in Cranberry, a northern suburb of Pittsburgh located in the neighboring Butler county. In the downtown Pittsburgh area, the contribution from biomass burning accounts for 7% of the PM_{2.5}. This source shows the highest variability with a standard deviation of 0.5 $\mu\text{g m}^{-3}$.

The maximum contribution of 8.05 $\mu\text{g m}^{-3}$ from industry is predicted near a cluster of industrial facilities in the town of ~~Butler~~Beaver, 37 km northwest of Pittsburgh. The maximum PM_{2.5} concentration of the modeling domain is located here. In this location long-range transport contributes 37% of the PM_{2.5} followed by industrial sources with 49% and biomass burning with 7%. On average, the contribution from industrial sources is low with 3.7%. In downtown Pittsburgh, the contribution is lower still with 2%.

On-road traffic emissions are most important in major highway intersections and river crossings surrounding downtown Pittsburgh with a maximum contribution of 3.9 $\mu\text{g m}^{-3}$ accounting for 24% of the PM_{2.5} in this area. On average, on-road traffic contributes 2.5% of the PM_{2.5} mass. The contribution from on-road traffic shows higher variability (standard deviation: 0.36 $\mu\text{g m}^{-3}$) since this sector contributes significantly to areas adjacent to the network of highways that radiates from the Pittsburgh downtown.

On average, commercial cooking emissions contribute 0.7% of the $PM_{2.5}$ in the modeling domain with a maximum contribution of $2.44 \mu g m^{-3}$ in downtown Pittsburgh, with smaller contributions in the surrounding urban area. Cooking is predicted to account for 16% of the $PM_{2.5}$ mass in downtown Pittsburgh. The contribution from commercial cooking is localized around downtown Pittsburgh and therefore shows little variability throughout the domain with a standard deviation of $0.1 \mu g m^{-3}$.

The miscellaneous area source sector contributes 6% of the $PM_{2.5}$ on average. Since this sector encompasses a variety of sources and activities, its contribution shows significant variability with a standard deviation of $0.34 \mu g m^{-3}$. The maximum contribution is located in the Pittsburgh urban core with $1.64 \mu g m^{-3}$, accounting for 11% of the $PM_{2.5}$.

The power generation sector contributes a maximum of $0.63 \mu g m^{-3}$ in the plume of the Bruce Mansfield power plant northwest of Pittsburgh ([this plant is no longer operating as of 2019](#)). ~~The contribution of this~~ sector shows the smallest variability ~~with at~~ $0.09 \mu g m^{-3}$. ~~The contribution to ground $PM_{2.5}$ mass from power generation in the winter are notably~~ relatively low-very small when compared with that in the summer period. ~~This is largely due to the height of the emissions stacks associated with this sector. A significant fraction of the emissions from power generation is trapped above the shallow mixing height in the winter, and much of the $PM_{2.5}$ mass is predicted to remain in the upper air layers. A map of the predicted relative high upper air $PM_{2.5}$ concentration from power generation are shown in Figure S5. can be found in the supplementary material (Figure S4).~~

Long-range transport from outside the inner modeling domain is the major source of $PM_{2.5}$ during this period contributing an average of 74%. This contribution varies from $7.1 \mu g m^{-3}$ in the southeast corner of the domain decreasing in the direction of the Pittsburgh urban core where the contribution is reduced to $5.9 \mu g m^{-3}$. In areas where there are significant local emissions such as the Pittsburgh downtown, the contribution from long-range transport decreases to 38%.

Contributions for all remaining sources are largest in the Pittsburgh downtown with $0.74 \mu g m^{-3}$, accounting for 5% of the $PM_{2.5}$. This sector also significantly contributes on the Ohio and Monongahela river valleys, where there is important rail and river traffic. On

average, these sources contribute 3% of the $PM_{2.5}$ and show a moderate variability with a standard deviation of $0.1 \mu g m^{-3}$.

For all local sources, the minimum contribution is close to zero (less than $0.1 \mu g m^{-3}$) and is located at the southwestern corner of the domain, near the Ohio – West Virginia border.

5. $PM_{2.5}$ concentrations and sources during summer

5.1 Effect of grid resolution

The predicted $PM_{2.5}$ concentrations in the simulated summer period are lower than during the winter period and more uniform, however, the qualitative behavior of the model at the different scales remains the same (Figure 6). Variable concentration limits are again used in these maps to remove background and highlight the effects of local sources. The standard deviation of the $PM_{2.5}$ increases from $0.28 \mu g m^{-3}$ at 36×36 , to $0.57 \mu g m^{-3}$ at 12×12 , to $0.72 \mu g m^{-3}$ at 4×4 and to $0.82 \mu g m^{-3}$ at 1×1 km. At the finest scale, the predicted variability in the summer is 61% of that in the winter. Similar to the winter period, the predicted maximum $PM_{2.5}$ concentration changes significantly with increasing resolution. The predicted maximum $PM_{2.5}$ increases from $6.4 \mu g m^{-3}$ at the coarse to $15.3 \mu g m^{-3}$ at the fine resolution. The finest scale better resolves the concentration field in the cluster of industrial installations 37 km northwest of Pittsburgh. The minimum $PM_{2.5}$ drops from $6.5 \mu g m^{-3}$ at 36×36 to $5.3 \mu g m^{-3}$ at 12×12 , and then to $4.7 \mu g m^{-3}$ at 1×1 km. As in the winter period, the moderate resolution appears to capture the majority of the concentration change from increasing resolution (67%).

The average EC is lower during the summer with $0.28 \mu g m^{-3}$ versus $0.43 \mu g m^{-3}$ in the winter. The standard deviation of the predicted average EC increases from $0.06 \mu g m^{-3}$ at 36×36 , to $0.09 \mu g m^{-3}$ at 12×12 , to $0.11 \mu g m^{-3}$ at 4×4 km, and to $0.13 \mu g m^{-3}$ at 1×1 km. The peak average EC is located in downtown Pittsburgh and increases by a factor of 3.6 (from 0.35 to $1.27 \mu g m^{-3}$) moving from the coarse to the finest resolution. It is noteworthy that the peak is 38% less than that of the winter when the coarse resolution is used, but only 21% when the finest resolution is used. The concentration range (difference between the maximum and the minimum) increases from $0.13 \mu g m^{-3}$ to $1.12 \mu g m^{-3}$ moving from the coarse to the finest resolution. This increase by a factor of 8.6 shows the

importance of the local variations of a primary species like EC in an urban area in both summer and winter.

The OA concentration field is quite uniform at the coarse-scale varying by only $0.17 \mu\text{g m}^{-3}$ (from 1.72 to $1.89 \mu\text{g m}^{-3}$) with a standard deviation of $0.07 \mu\text{g m}^{-3}$ (Figure 6). Variability increases significantly when one moves to the finest scale, with the range increasing to $2.24 \mu\text{g m}^{-3}$ (from 1.55 to $3.79 \mu\text{g m}^{-3}$) and the standard deviation of the OA field increases to $0.2 \mu\text{g m}^{-3}$. The use of the finest scale appears to be needed for the resolution of the OA high concentration areas in the summer more than in the winter.

The $\text{PM}_{2.5}$ sulfate levels during the summer period are on average 12% higher during the summertime period. At the coarse and intermediate scales, the predicted average concentration fields have relatively little structure (Figure 7). The corresponding concentration ranges are relatively narrow ($0.05 \mu\text{g m}^{-3}$ at $36 \times 36 \text{ km}$ and $0.42 \mu\text{g m}^{-3}$ at $12 \times 12 \text{ km}$). However, a different picture emerges at the fine and especially the finest scales. The plumes from the major power plants can be clearly seen at these higher resolutions. The maximum increased by $0.5 \mu\text{g m}^{-3}$ from the coarse scale to the finest scale while the minimum is reduced from $1.78 \mu\text{g m}^{-3}$ at 36×36 to $1.05 \mu\text{g m}^{-3}$ at 12×12 , to $0.95 \mu\text{g m}^{-3}$ at 4×4 and $1 \times 1 \text{ km}$. The standard deviation of the predicted sulfate concentration field at the coarse resolution is low and similar to that in winter, $0.02 \mu\text{g m}^{-3}$. However, the variability at the finest scale in the summer ($0.13 \mu\text{g m}^{-3}$ at $1 \times 1 \text{ km}$) is twice the predicted variability in the winter.

The predicted summertime nitrate concentrations are quite low in the area (average $0.5 \mu\text{g m}^{-3}$ in the coarse and $0.46 \mu\text{g m}^{-3}$ in the finest resolution). The predicted minimum decreases from $0.42 \mu\text{g m}^{-3}$ at 36×36 to $0.39 \mu\text{g m}^{-3}$ at 12×12 , to $0.34 \mu\text{g m}^{-3}$ at 4×4 , and to $0.3 \mu\text{g m}^{-3}$ at $1 \times 1 \text{ km}$. The predicted maximum concentration increases from $0.56 \mu\text{g m}^{-3}$ at the coarse scale to $0.71 \mu\text{g m}^{-3}$ at the intermediate scale and stays relatively constant at higher resolutions. The concentration field is quite uniform with a standard deviation ranging from 0.06 to $0.09 \mu\text{g m}^{-3}$ for all scales. However, due to the reduction in the predicted minimum the concentration range increases from $0.14 \mu\text{g m}^{-3}$ at the coarse resolution to $0.37 \mu\text{g m}^{-3}$ at the finest resolution.

The PM_{2.5} ammonium concentration field is quite uniform at all resolutions (Figure 7). The concentration range increases from 0.04 to 0.22 $\mu\text{g m}^{-3}$ moving from the coarse to the finest resolution and the standard deviation increases from 0.02 to 0.04 $\mu\text{g m}^{-3}$.

5.2 Source Apportionment

The local emissions for each source category in July 2017 are shown in Table 2. During summer, residential biomass burning is minimal. This source contributes a maximum of 0.04 $\mu\text{g m}^{-3}$ and an average of 0.007 $\mu\text{g m}^{-3}$, accounting for 0.6% of the average total PM_{2.5}.

Power generation sources have the highest average contribution to total PM_{2.5} of all the local sources of 10%. Industrial sources account for 6% of the average PM_{2.5} but are the most important contributor in the point of the modeling domain with the maximum predicted PM_{2.5} concentration. At this location in Butler-Beaver County, industrial sources account for 58% of total PM_{2.5}.

As in the winter period, on-road traffic emissions have the largest contribution to the PM_{2.5} in the downtown Pittsburgh area where four large highways intersect. In this location on-road traffic contributes 26% of the PM_{2.5}. On average, local on-road traffic contributes around 3% of the PM_{2.5} mass. During the summer period, the variability of the on-road traffic contribution is slightly lower with 0.33 $\mu\text{g m}^{-3}$ compared with 0.36 $\mu\text{g m}^{-3}$ during winter.

Commercial cooking emissions contribute a maximum of 2.08 $\mu\text{g m}^{-3}$ to the average total PM_{2.5} in downtown Pittsburgh. This source accounts for 17% of the PM_{2.5} in the city but only 1% for the entire modeling domain. The large predicted contribution from cooking PM_{2.5} is consistent with the mobile AMS measurements performed by Ye et al. (2018), where it was determined that indicated that cooking organic aerosol contributes up to 60% of the non-refractory PM₁ mass. Mobile AMS results from Gu et al. (2018) showed that cooking OA contributes 5-20% of PM₁ mass over multiple areas in the city of Pittsburgh. Other measurements in Pittsburgh also showed that cooking OA concentrations were clearly elevated in the vicinity of restaurants when compared with residential areas (Robinson et al., 2018). Though the average cooking PM_{2.5} mass predictions offrom our studyPMCAMx cannot be directly compared to these numbersmeasurements, they all is

~~body of previous work highlights the local importance of cooking as a fine PM pollution source. Other measurements in Pittsburgh showed that cooking OA concentrations were clearly elevated in the vicinity of restaurants when compared with residential areas (Robinson et al., 2018).~~

On average, the miscellaneous area sources sector contributes $0.26 \mu\text{g m}^{-3}$ accounting for 4.3% of the $\text{PM}_{2.5}$. In downtown Pittsburgh, where the contribution is highest, this source contributes 7% of the $\text{PM}_{2.5}$.

Unlike in the winter period, the plumes from major powerplants in the Ohio river valley are clearly resolved in the summer. The power generation sector contributes a maximum of $2.4 \mu\text{g m}^{-3}$ in the plume of the Bruce Mansfield power plant northwest of Pittsburgh. On average, the 9.4% contribution from this sector to the $\text{PM}_{2.5}$ is much larger than in the winter where it only contributed 2.3%. The plume from the Mitchell power plant in the southwest corner of the modeling domain is clearly resolved and reaches all the way to the city. This increases the contribution from power generation to the $\text{PM}_{2.5}$ in the downtown core from $0.22 \mu\text{g m}^{-3}$ in the winter to $0.61 \mu\text{g m}^{-3}$ in the summer. The maximum contribution of $8.98 \mu\text{g m}^{-3}$ from industrial sources is a cluster of industrial facilities in the town of ~~Butler~~Beaver, northwest of Pittsburgh.

Long-range transport from sources outside the region contributes a maximum of $5.2 \mu\text{g m}^{-3}$ in the southeast corner of the domain decreasing in the direction of the Pittsburgh northern suburbs where the contribution is minimal with $4.1 \mu\text{g m}^{-3}$. On average, long-range transport accounts for 72% of the $\text{PM}_{2.5}$ mass. In downtown Pittsburgh, long-range transport contributes $4.24 \mu\text{g m}^{-3}$ accounting for 35% of the $\text{PM}_{2.5}$. The high-concentration spot area visible on the western edge of the domain is due to a cluster of power generation and industrial sources located in the Ohio River valley just outside of the inner modeling domain.

On average, the contribution from all remaining sources is 3.6% and shows a moderate variability of $0.10 \mu\text{g m}^{-3}$. The contribution from these sources is maximal in downtown Pittsburgh with $0.78 \mu\text{g m}^{-3}$ accounting for 6% of the $\text{PM}_{2.5}$.

For all local sources, the minimum contribution is close to zero (less than $0.1 \mu\text{g m}^{-3}$) and is located at the northwestern corner of the domain, near the Ohio – Pennsylvania border.

Relative contributions of all local sources to domain average predicted total PM_{2.5} (including long-range transport PM_{2.5} mass) are shown in Figure 9. The largest differences between February and July are the contributions from biomass burning and power generation. In the winter, biomass burning is the most important local source of PM_{2.5}, contributing over 8%. In the summer, this source contributes much less than 1% to total PM_{2.5}. This discrepancy can easily be explained by the lack of residential wood combustion in the warmer months of the year. Power generation is a significantly more important source in July than in February. This is likely a result of a lower mixing height in the winter combined with emissions plumes from power plants in the Ohio river valley originating from very tall stacks.

The relative contributions of local sources to average predicted total PM_{2.5} in the maximum concentration cell in [Butler-Beaver](#) County and in downtown Pittsburgh are shown in Figures 10 and 11, respectively. The dominant local source in the [Butler-Beaver](#) County location is industrial emissions, due to the proximity of various industrial installations in this area. Industrial sources here account for around 49% of total PM_{2.5} in February and 58% of total PM_{2.5} in July. A lot of the difference in industrial PM_{2.5} at the [Butler-Beaver](#) County location between months is made up by biomass burning in February, which accounts for 7% more of the total compared to July. [In the downtown area of Pittsburgh, the majority of PM_{2.5} from local sources can be attributed to either traffic \(22-27% of total PM_{2.5}\) or cooking \(16-18% of total PM_{2.5}\) in both simulation periods \(Figure 11\).](#)

6. Exposure to PM_{2.5}

The population data in the inner domain from the 2010 U.S. census was used to estimate the exposure of the population in the Pittsburgh area to model predictions of PM_{2.5} during winter of 2017 at the different grid resolutions. We ranked the average PM_{2.5} concentrations from all the cells in the modeling domain and created bins of 0.2 µg m⁻³. A sum of the population from all the grid cells that fall within each concentration bin was calculated and divided by the total population of the inner grid to construct population exposure histograms. [The population data used here is resolved at the census group level, which is much smaller than the simulation grid cell size of 1 x 1 km.](#)

6.1 Winter PM_{2.5} Exposure

Figure 12 shows the population exposure histograms for the Pittsburgh area (inner domain) for each model resolution. At the coarse resolution, there are only four PM_{2.5} values and 46% of the population is exposed to a concentration of 10.4 $\mu\text{g m}^{-3}$ with decreasing exposure with PM_{2.5} concentration. At a 12 km resolution, the low concentration side of the distribution is better resolved but gaps can still be observed at higher levels. At this intermediate resolution, the largest fraction of the population (15%) is exposed to PM_{2.5} concentrations of 11.8 $\mu\text{g m}^{-3}$.

When the resolution is increased to 4 km the biggest improvements on the model ability to resolve the exposure distribution happen at concentrations higher than 9.4 $\mu\text{g m}^{-3}$. At the fine resolution, no gaps appear in the distribution. A maximum of 12% of the population is exposed to PM_{2.5} concentrations of 12 $\mu\text{g m}^{-3}$ while at the highest concentration of 12.8 $\mu\text{g m}^{-3}$ 3% are exposed. At the 1 km resolution, the distribution is much smoother due to the ability of this finest grid to capture local gradients. The largest fraction of the population (6%) is exposed to PM_{2.5} concentrations of 9.2 $\mu\text{g m}^{-3}$. At the highest concentration of 14.4 $\mu\text{g m}^{-3}$ the exposed population is less than 0.1% as this maximum point is located near industrial installations 37 km northwest of Pittsburgh where the population density is very low.

The differences seen between the predicted exposure distributions at 4 km and 1 km resolutions highlight the need for high resolution modeling studies in order to identify key areas from an environmental justice perspective. The upper tail of the exposure distribution (13-14 $\mu\text{g m}^{-3}$) is only detectable visible at with the 1 km resolution predictions. These higher exposures could be addressed by appropriate targeted also have the ability to be alleviated by appropriate regulations, because they are thea direct result of proximity to either major industrial sources- and and electrical generation sources or dense traffic and cooking emissions. -stations.

At resolutions of 36 km, 12 km, 4 km, and 1 km the predicted average population weighted total PM_{2.5} concentration during February 2017 is 9.74 $\mu\text{g m}^{-3}$, 9.77 $\mu\text{g m}^{-3}$, 10.28 $\mu\text{g m}^{-3}$, and 10.00 $\mu\text{g m}^{-3}$, respectively. This represents an increase of only 2.6% when moving from lowest to highest resolution. Relative contributions of local sources to

average population weighted PM_{2.5} concentration is shown in Figure 14. Compared to the domain average PM_{2.5} concentrations (Figure 9), many local source contributions are enhanced in terms of average population exposure. In February, weighting PM_{2.5} concentrations by population increases the contribution from biomass burning from 8.3% to 11.7%. Other notable increases include onroad traffic (2.5% to 6.5%), and miscellaneous area sources (5.9% to 9.2%). Other local source contributions to population weighted PM_{2.5} were similar to the corresponding non-weighted concentrations.

The source-resolved population exposure distributions during this winter period are shown in Figures S6 and S7.

6.2 Summer PM_{2.5} Exposure

Figure 134 shows the population exposure for each simulation grid during the summer period. At the coarse resolution, 88% of the population is exposed to a concentration of 7 to 7.2 $\mu\text{g m}^{-3}$. At 12 x 12 km resolution, the exposure distribution is better resolved but a gap is still present at 7.2 $\mu\text{g m}^{-3}$ and exposure to PM_{2.5} concentrations above 7.6 $\mu\text{g m}^{-3}$ is not resolved at all. At this intermediate resolution, the largest fraction of the population (19%) is exposed to PM_{2.5} concentrations of 7.4 $\mu\text{g m}^{-3}$. Increasing the resolution to 4 x 4 km both shifts the distribution to slightly lower concentrations and resolves exposure to higher PM_{2.5} concentrations than with the 12 x 12 km grid. At this resolution, 14% of the population is exposed to 6.4 $\mu\text{g m}^{-3}$ and smaller portions of the population are exposed to concentrations higher than 8.0 $\mu\text{g m}^{-3}$. Moving to the highest resolution grid further resolves the exposure distribution. Most notably, 1 x 1 km resolution reveals a bimodal distribution of population exposure, with one peak centered around 6.0 $\mu\text{g m}^{-3}$ and another centered around 7.4 $\mu\text{g m}^{-3}$. This likely corresponds to one subset of the population in the urban areas of Pittsburgh who are exposed to higher PM_{2.5} concentrations and another subset representing the surrounding suburban areas.

In the summer period, an even larger range of high-concentration exposure is revealed moving from 4 km to 1 km resolution. At this high resolution, the Here, we gain information about population exposure to concentrations ranging from 8.5 $\mu\text{g m}^{-3}$ to 12 $\mu\text{g m}^{-3}$ becomes clear Most people exposed to these higher fine PM levels according to PMCAMx . Again, this corresponds to people living in the vicinity of the industrial

complexes and power stations around the city of Beaver. The higher concentration range of the upper tail of the exposure during in July compared to February is due to a large extent to the effective mixing of the emissions from the tall stacks down to the ground level-2017 is likely a consequence of the higher level of power generation PM_{2.5} in the ground level simulation layer compared to that seen in February 2017.

At resolutions of 36 km, 12 km, 4 km, and 1 km the predicted average population weighted total PM_{2.5} concentration during February 2017 is 7.06 $\mu\text{g m}^{-3}$, 6.78 $\mu\text{g m}^{-3}$, 7.00 $\mu\text{g m}^{-3}$, and 6.99 $\mu\text{g m}^{-3}$, respectively. This represents just a 1% decrease between the lowest and highest resolutions. Similar to the effect seen in February, weighting PM_{2.5} concentrations by population increases the contribution from onroad traffic from 3.3% to 8.9% in July. Contributions from miscellaneous area sources also increased (4.3% to 7.1%) when weighting by population. The population weighted contribution from power generation sources in July decreased from the non-weighted value from 9.4% to 8.3%. All other local source contributions to population weighted PM_{2.5} in July were similar to the non-weighted values.

The source-resolved population exposure distributions during this summer period are shown in Figures S8 and S9.

7. Conclusions

We applied the PMCAMx chemical transport model over the city of Pittsburgh for the simulation periods of February and July 2017 using a series of telescoping grids at 36 x 36 km, 12 x 12 km, 4 x 4 km and 1 x 1 km. Emissions were calculated using 2017 projections from the 2011 NEI. Emissions were distributed geographically using the spatial surrogates provided with the NEI11 for all grids. For commercial cooking, a new 1 x 1 km spatial surrogate was developed using restaurant count data from the Google Places API. Traffic model data was used to develop a 1 x 1 km spatial surrogate for on-road traffic emissions.

At the coarse resolution, county-level differences can be observed. Increasing the resolution to 12 x 12 km resolves the urban-rural gradient and further increasing to 4 x 4 resolves large stationary sources such as power plants. Only at the finest resolution intra-urban variations and individual roadways are resolved. Low variability, regional pollutants

such as nitrate show limited improvement after increasing the resolution to 12 x 12 km while predominantly local pollutants such as elemental carbon and winter organic aerosol have gradients that can only be resolved at the finest resolution.

Biomass burning shows the largest variability during the winter period with many local maxima and significant emissions within the city and in the suburbs. During the summer contributions from this source are negligible. In contrast with the winter period, during the summer the plumes from large power plants in the Ohio river valley can be resolved. These plumes are rich in sulfates and start being resolved at 4 x 4 km with significant detail added at 1 x 1 km. During both periods the largest contributing source to the average PM_{2.5} is particles from outside the modeling domain.

The ability of the model to resolve the exposure distribution increases at different rates according to the concentration. A significant improvement in resolving exposure to concentrations below 9.4 µg m⁻³ in the winter and below 7.0 µg m⁻³ in the summer is achieved by increasing the resolution to 12 x 12 km. Only at the finest resolution is the exposure to concentrations above 9.6 µg m⁻³ in the winter and above 8.6 µg m⁻³ in the summer fully resolved as well as the impact of high concentration spots.

The average exposure in terms of average contribution to population weighted PM_{2.5} concentrations of some local sources is enhanced compared to the non-weighted average PM_{2.5} concentrations. In February, weighting by population enhanced the contributions from biomass burning, onroad traffic, and miscellaneous area sources by 3-4%. In July, the contributions from onroad traffic and miscellaneous area sources also increased by 3-5% from this procedure.

It was determined that increasing simulation grid resolution from 36 x 36 km to 1 x 1 km had minimal effect on the predicted domain average population weighted PM_{2.5} concentration. Moving from the lowest to highest grid resolution increased the predicted average population weighted PM_{2.5} by less than 3%. In July, the average decreased by 1%. This negligible change in the predicted average exposure to PM_{2.5} suggests that extremely high resolution predictions of urban PM_{2.5} pollution may not be necessary for accurate epidemiological analysis in the absence of high-resolution health data. ~~However it is also clear that the~~ average population-weighted concentration approach misses the potentially important ~~ignores the~~ impacts of large sources on smaller communities. ~~The~~

increased neighborhood scale resolution ~~could be~~ is vital for ~~topics related to environmental justice—~~identifying communities that are disproportionately exposed to large ~~stationary~~ sources of PM_{2.5} pollution, which in our study represent the upper tail of the exposure distributions in both simulation periods.

8. Code and data availability

The code and simulation results are available upon request (spyros@chemeng.upatras.gr).

9. Supplement

10. Author contributions

P.G.R. and B.T.D. performed the PMCAMx simulations, analyzed the results and wrote the manuscript. P.G.R. prepared the anthropogenic emissions and other inputs for the simulations. I.K. set-up the WRF simulations and assisted in the preparation of the meteorological inputs. S.N.P. and P.J.A. designed and coordinated the study and helped in the writing of the paper. All authors reviewed and commented on the manuscript.

11. Competing interests

The authors declare that they have no conflict of interest.

12. Financial Support

This work was supported by the Center for Air, Climate, and Energy Solutions (CACES) which was supported under Assistance Agreement No. R835873 awarded by the U.S. Environmental Protection Agency and the Horizon-2020 Project REMEDIA of the European Union under grant agreement No 874753.

13. References

- Anand, S.: The concern for equity in health. *Journal of Epidemiology & Community Health* 56, 485–487, 2002.
- Arunachalam, S., Holland, A., Do, B., Abraczinskas, M.: A quantitative assessment of the influence of grid resolution on predictions of future-year air quality in North Carolina, USA. *Atmospheric Environment* 40, 5010–5026, 2006.
- Carter, W. P. L.: Documentation of the SAPRC-99 chemical mechanism for VOC reactivity assessment, 1999.
- Day, M., Pouliot, G., Hunt, S., Baker, K.R., Beardsley, M., Frost, G., Mobley, D., Simon, H., Henderson, B., Yelverton, T., Rao, V.: Reflecting on progress since the 2005 NARSTO emissions inventory report. *Journal of the Air & Waste Management Association* 69, 1025–1050, 2019.
- Dockery, D. W., Pope, C. A.: Acute respiratory effects of particulate air pollution. *Annual Review of Public Health* 15, 107–132, 1994.
- [Donahue N. M.; Robinson, A. L.; Stanier, C. O.; Pandis, S. N.: Coupled partitioning, dilution, and chemical aging of semivolatile organics. *Environmental Science & Technology*, 40, 2635-2643, 2006.](#)
- Elessa Etuman, A., Coll, I.: OLYMPUS v1.0: Development of an integrated air pollutant and GHG urban emissions model-methodology and calibration over greater Paris. *Geoscientific Model Development* 11, 5085–5111, 2018.
- [ENVIRON: CAMx \(Comprehensive Air Quality Model with Extensions\) User's Guide Version 4.20, 2005.](#)
- Eyth, A., Vukovich, J.: Technical Support Document (TSD): Preparation of Emissions Inventories for the Version 6.2, 2011 Emissions Modeling Platform, 2016.
- [Fahey, K. M.; Pandis, S. N.: Optimizing model performance: variable size resolution in cloud chemistry modeling. *Atmospheric Environment*, 35, 4471-4478, 2001.](#)
- Fountoukis, C., Koraj, D., Denier van der Gon, H. A. C., Charalampidis, P. E., Pilinis, C., Pandis, S. N.: Impact of grid resolution on the predicted fine PM by a regional 3-D chemical transport model. *Atmospheric Environment* 68, 24–32, 2013.
- Fountoukis, C., Racherla, P. N., Denier van der Gon, H. A. C., Polymeneas, P., Charalampidis, P. E., Pilinis, C., Wiedensohler, A., Dall'Osto, M., O'Dowd, C.,

- Pandis, S. N.: Evaluation of a three-dimensional chemical transport model (PMCAMx) in the European domain during the EUCAARI May 2008 campaign. *Atmospheric Chemistry and Physics* 11, 10331–10347, 2011.
- Gilliam, R. C., Pleim, J. E.: Performance assessment of new land surface and planetary boundary layer physics in the WRF-ARW. *Journal of Applied Meteorology and Climatology* 49, 760–774, 2010.
- Gu, P., Li, H. Z., Ye, Q., Robinson, E. S., Apte, J. S., Robinson, A. L., Presto, A. A.: Intracity variability of particulate matter exposure is driven by carbonaceous sources and correlated with land-use variables. *Environmental Science and Technology* 52, 11545–11554, 2018.
- Hogrefe, C., Pouliot, G., Wong, D., Torian, A., Roselle, S., Pleim, J., Mathur, R.: Annual application and evaluation of the online coupled WRF-CMAQ system over North America under AQMEII phase 2. *Atmospheric Environment* 115, 683–694, 2015.
- [Karydis, V. A.,[‡] Tsimpidi, A. P.,[‡] Fountoukis, C.,[‡] Nenes, A.,[‡] Zavala, M.,[‡] Lei, W.,[‡] Molina, L. T.,[‡] Pandis, S. N.: Simulating the fine and coarse inorganic particulate matter concentrations in a polluted megacity. *Atmospheric Environment* 44, 608–620, 2010.](#)
- Kumar, N., Russell, A. G.: Multiscale air quality modeling of the Northeastern United States. *Atmospheric Environment* 30, 1099–1116, 1996.
- Lane, T. E., Donahue, N. M., Pandis, S. N.: Effect of NO_x on secondary organic aerosol concentrations. *Environmental Science & Technology* 42, 6022–6027, 2008.
- Ma, W., Pi, X., Qian, S.: Estimating multi-class dynamic origin-destination demand through a forward-backward algorithm on computational graphs. *Transportation Research Part C: Emerging Technologies*, 119, 102747, doi:10.1016/j.trc.2020.102747, 2020.
- McDonald, B., McBride, Z.: High-resolution mapping of motor vehicle carbon dioxide emissions. *Journal of Geophysical Research*, 119, 5283–5298, 2014.
- [Murphy, B. N.,[‡] Pandis, S. N.: Simulating the formation of semivolatile primary and secondary organic aerosol in a regional chemical transport model. *Environmental Science & Technology*, 43, 4722–4728, 2009.](#)
- [Nenes A.,[‡] Pandis, S. N.,[‡] Pilinis, C.: ISORROPIA: A new thermodynamic equilibrium](#)

- [model for multiphase multicomponent inorganic aerosols. *Aquatic Geochemistry*, 4, 123-152, 1998.](#)
- Pan, S., Choi, Y., Roy, A., Jeon, W.: Allocating emissions to 4 km and 1 km horizontal spatial resolutions and its impact on simulated NO_x and O₃ in Houston, TX. *Atmospheric Environment* 164, 398–415, 2017.
- Pandis, S. N., Wexler, A. S., Seinfeld, J. H.: Secondary organic aerosol formation and transport - II. Predicting the ambient secondary organic aerosol size distribution. *Atmospheric Environment*, 27, 2403–2416, 1993.
- Robinson, E. S., Gu, P., Ye, Q., Li, H. Z., Shah, R. U., Apte, J. S., Robinson, A. L., Presto, A. A.: Restaurant impacts on outdoor air quality: Elevated organic aerosol mass from restaurant cooking with neighborhood-scale plume extents. *Environmental Science and Technology* 52, 9285–9294, 2018.
- Rogers, R. E., Deng, A., Stauffer, D. R., Gaudet, B. J., Jia, Y., Soong, S. T., Tanrikulu, S.: Application of the weather research and forecasting model for air quality modeling in the San Francisco bay area. *Journal of Applied Meteorology and Climatology* 52, 1953–1973, 2013.
- Seinfeld, J. H., Pandis, S. N.: *Atmospheric Chemistry and Physics: From Air Pollution to Climate Change*, 2nd. ed. John Wiley & Sons, Inc., Hoboken, 2006.
- Stroud, C. A., Makar, P. A., Moran, M. D., Gong, W., Gong, S., Zhang, J., Hayden, K., Mihele, C., Brook, J. R., Abbatt, J. P. D., Slowik, J. G.: Impact of model grid spacing on regional- and urban-scale air quality predictions of organic aerosol. *Atmospheric Chemistry and Physics* 11, 3107–3118, 2011.
- [Tsimpidi, A. P., Karydis, V. A., Zavala, M., Lei, W., Molina, L., Ulbrich, I. M., Jimenez, J. L., Pandis, S. N.: Evaluation of the volatility basis-set approach for the simulation of organic aerosol formation in the Mexico City metropolitan area. *Atmospheric Chemistry and Physics*, 10, 525-546, 2010.](#)
- [United States Environmental Protection Agency: 2011 National Emissions Inventory, version 2 Technical Support Document, 2015.](#)
- [Ye, Q., Gu, P., Li, H. Z., Robinson, E. S., Lipsky, E., Kaltsounoudis, C., Lee, A. K. Y., Apte, J. S., Robinson, A. L., Sullivan, R. C., Presto, A. A., Donahue, N. M.: Spatial variability of sources and mixing state of atmospheric particles in a](#)

[metropolitan area. Environmental Science & Technology, 52, 6807-6815, 2018.](#)

Zakoura, M., Pandis, S. N.: Improving fine aerosol nitrate predictions using a Plume-in-Grid modeling approach. Atmospheric Environment 116887, doi:10.1016/j.atmosenv.2019.116887, 2019.

Zakoura, M., Pandis, S. N.: Overprediction of aerosol nitrate by chemical transport models: The role of grid resolution. Atmospheric Environment 187, 390–400, 2018.

Table 1. PM_{2.5} emissions by source for the 1 x 1 km Pittsburgh domain (February 2017).

Source Type	Emissions (kg d ⁻¹ km ⁻²)								
	PM _{2.5}	OA	EC	Chl.	Na	Amm.	Nitrate	Sulfate	Other
Agricultural dust	68.7	9.7	0.4	0.2	0.1	0.1	0.1	0.7	57.2
River barges	19.0	4.2	14.7	0.0	0.0	0.0	0.0	0.1	0.1
Cooking	242	223	8.3	2.2	0.8	0.0	1.1	0.6	6.0
Misc. area sources	683	445	56.7	30.5	3.0	5.6	1.7	42	97.8
Off-road	147	56.2	73.1	0.3	0.1	0.0	0.3	1.1	16.1
Oil-gas (Area)	35.3	1.7	0.0	0.0	0.0	0.0	0.1	8.3	23.2
On-road traffic	188	84.6	75.2	0.3	0.1	1.8	0.6	8.3	16.4
Rail	40.7	8.9	31.4	0.0	0.0	0.0	0.0	0.1	0.2
Biomass burning	1,869	1,696	105	5.6	1.8	2.8	3.6	7.7	46.3
Power generation	3,517	201	194	2.8	0.0	15.7	2.6	460	2,641
Industrial	1,106	192	134	79.4	65.3	10.1	21.1	173	428
Oil-gas (point)	2.8	1.0	1.1	0.0	0.0	0.0	0.1	0.2	0.5

Table 2. PM_{2.5} emissions by source for the 1 x 1 km Pittsburgh domain (July 2017).

Source Type	Emissions (kg d ⁻¹ km ⁻²)								
	PM _{2.5}	OA	EC	Chl.	Na	Amm.	Nitrate	Sulfate	Other
Agricultural dust	67.3	8.9	0.4	0.1	0.1	0.1	0.1	0.7	56.9
River barges	19.0	4.2	14.7	0.0	0.0	0.0	0.0	0.1	0.1
Cooking	242	223	8.3	2.2	0.8	0.0	1.1	0.6	6
Misc. area sources	593	392	49.1	28.5	2.5	5.3	1.1	33	81.6
Off-road	205	83.5	92.9	0.2	0.1	0.0	0.4	1.1	27.3
Oil-gas (Area)	35.9	1.9	0.0	0.0	0.0	0.0	0.1	8.9	25.0
On-road traffic	162	67.6	66	0.4	0.1	1.5	0.5	8.6	17.2
Rail	40.7	8.9	31.4	0.0	0.0	0.0	0.0	0.1	0.2
Biomass burning	24.3	22	1.4	0.0	0.0	0.0	0.0	0.1	0.6
Power generation	3,780	216	208	3.1	0.0	16.9	2.8	495	2,840
Industrial	1,050	188	133	67.3	56.2	9.9	21.0	165	412
Oil-gas (point)	2.8	1.0	1.1	0.0	0.0	0.0	0.1	0.2	0.5

Table S1. Outer (CONUS) boundary condition concentrations of major aerosol species.

Component	Concentration ($\mu\text{g m}^{-3}$)			
	West	East	South	North
Nitrate	0.01	0.01	0.03	0.03
Ammonium	0.14	0.25	0.24	0.16
Sulfate	0.64	1.12	0.81	0.68
Elemental carbon	0.04	0.05	0.09	0.03
Organic aerosol (Winter)	0.20	0.16	0.58	0.80
Organic aerosol (Summer)	0.80	0.80	0.80	0.80

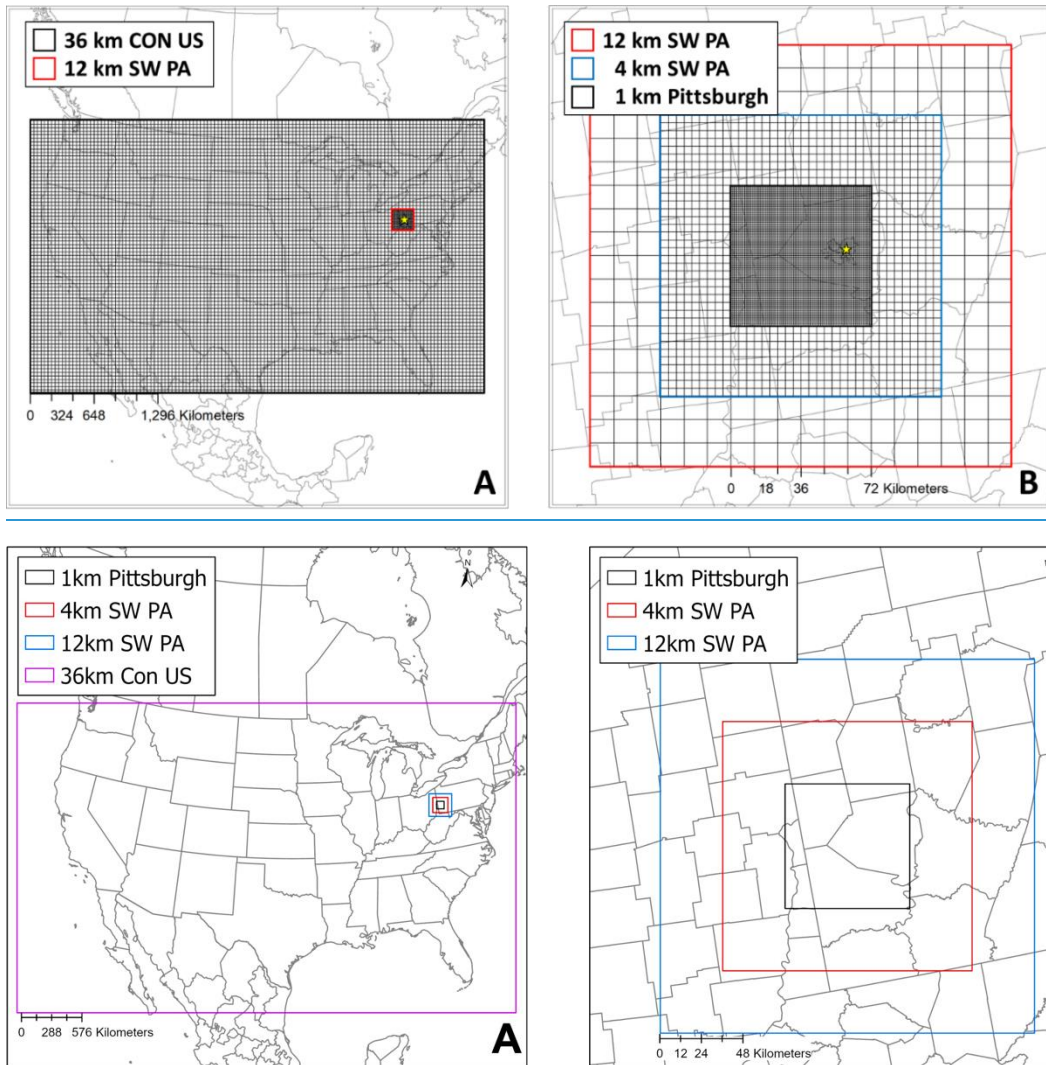


Figure 1. Modeling domain used for the PMCAMx simulations. (A) 36 x 36 km continental U.S. grid. (B) 12 x 12 and 4 x 4 km South Western Pennsylvania grids, and 1 x 1 km Pittsburgh nested grids.

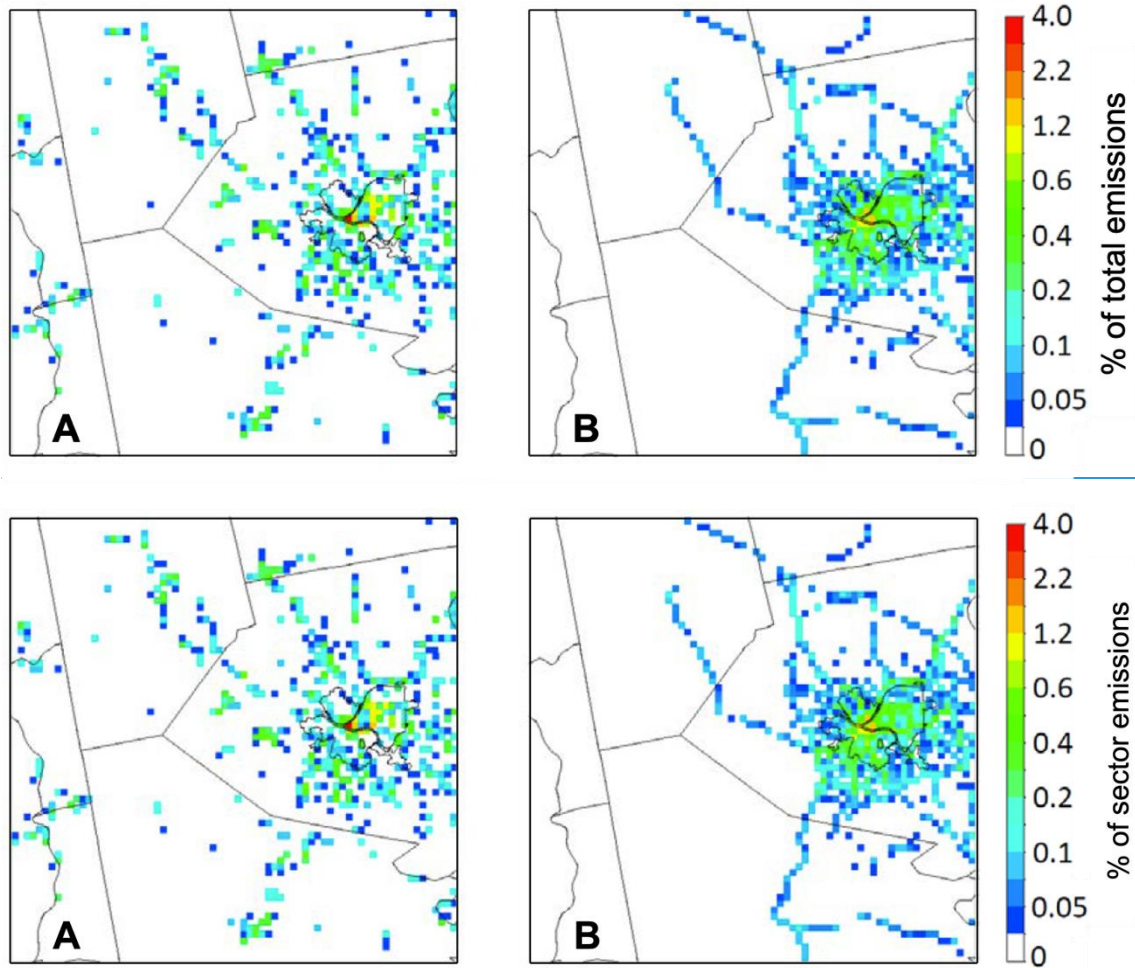


Figure 2. Percentage of [sector](#) PM_{2.5} emissions in each 1x1 km computational cell for: (A) commercial cooking and (B) on road traffic [in February 2017](#). [The value of the colored points in each framemap add up to unity4.0, corresponding to 100% of emissions for the respective sectors.](#)

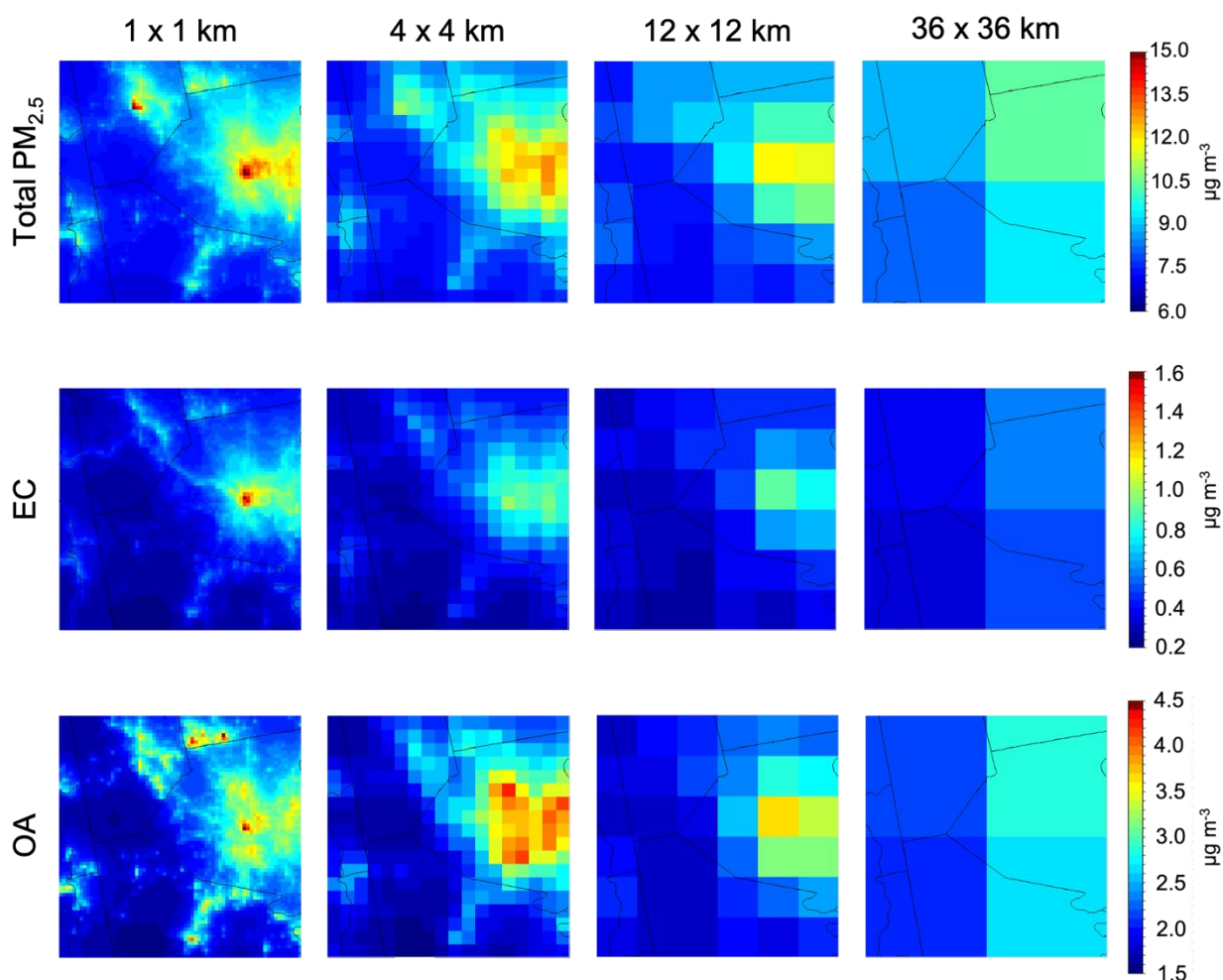
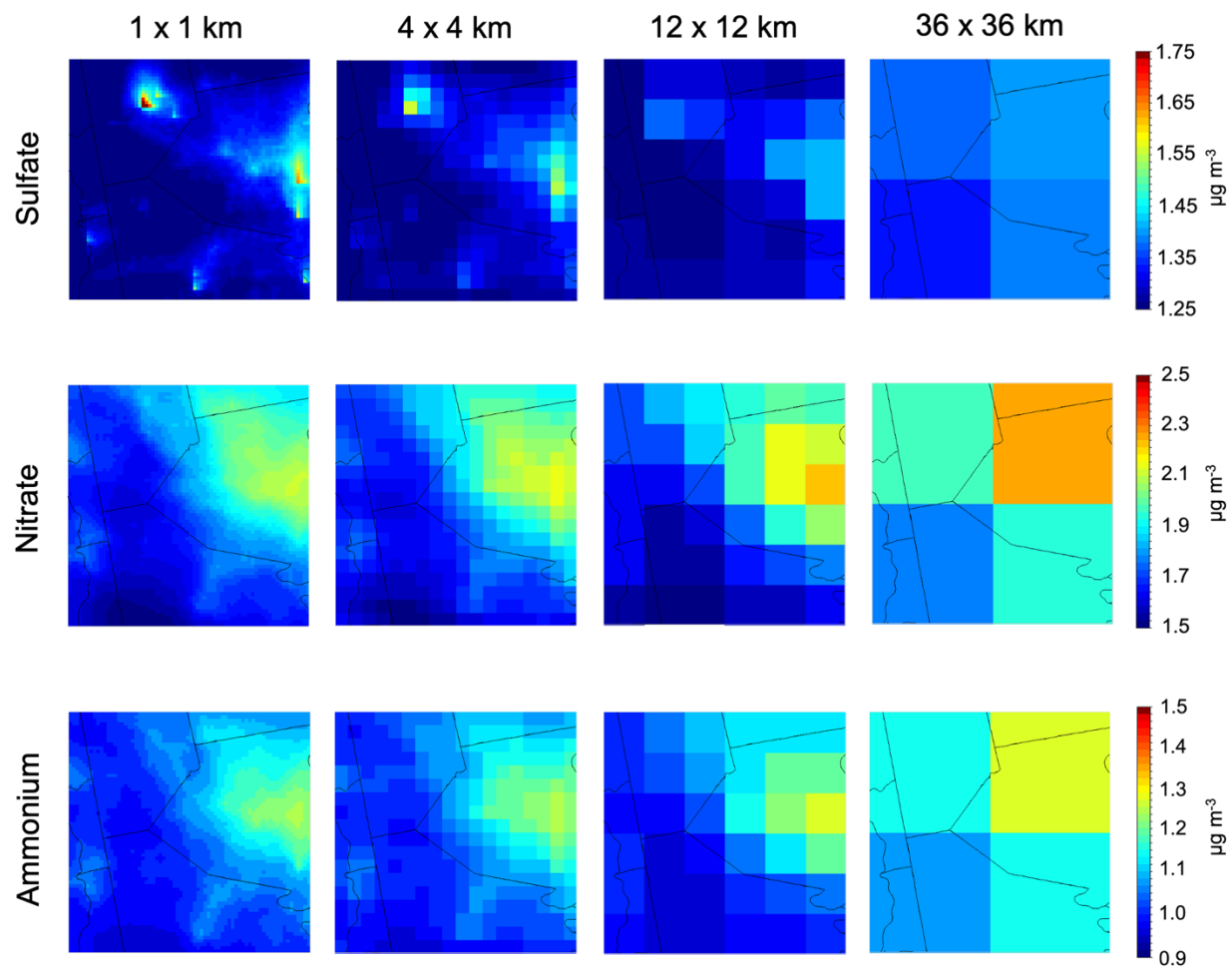


Figure 3. Average predicted ground-level concentration of total PM_{2.5}, EC, and OA at 36 x 36, 12 x 12, 4 x 4 and 1 x 1 km resolutions during February 2017. Different color scales that do not start from zero are used for the various maps.

777

778



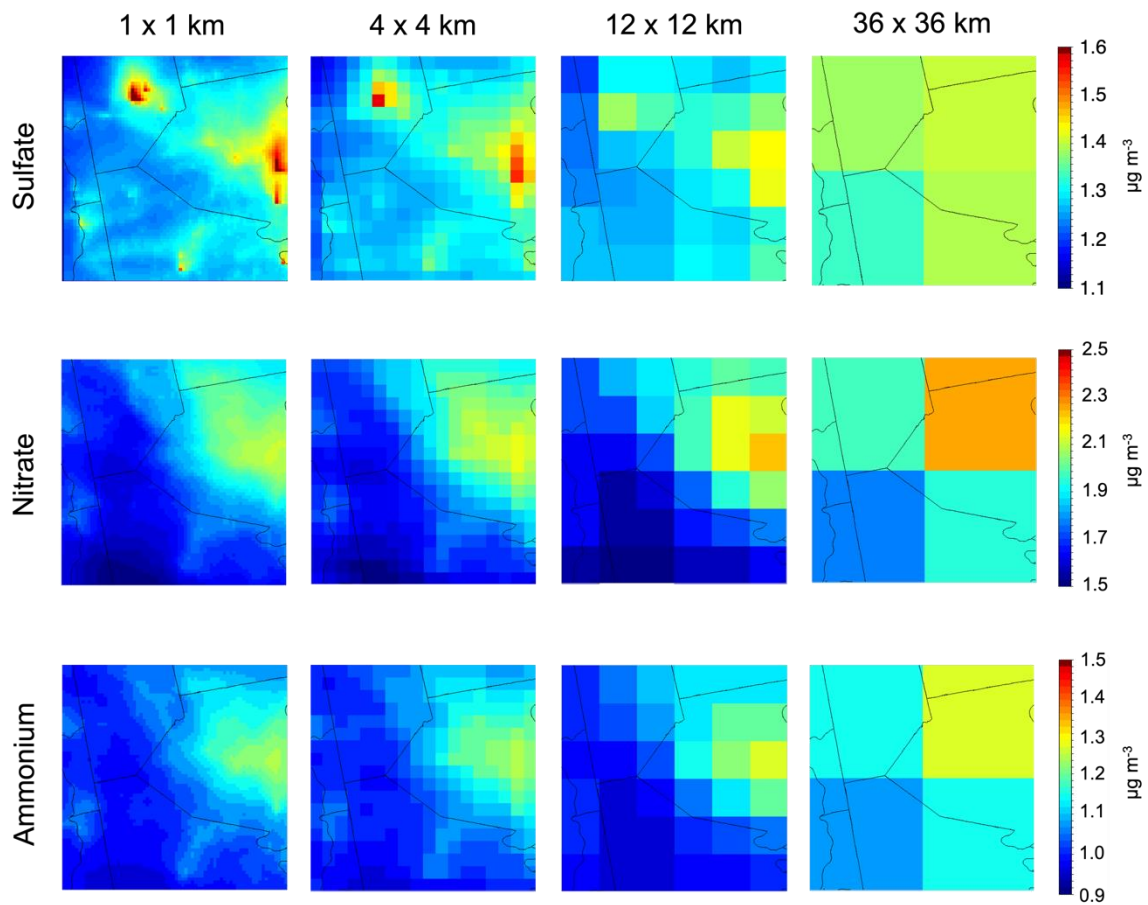
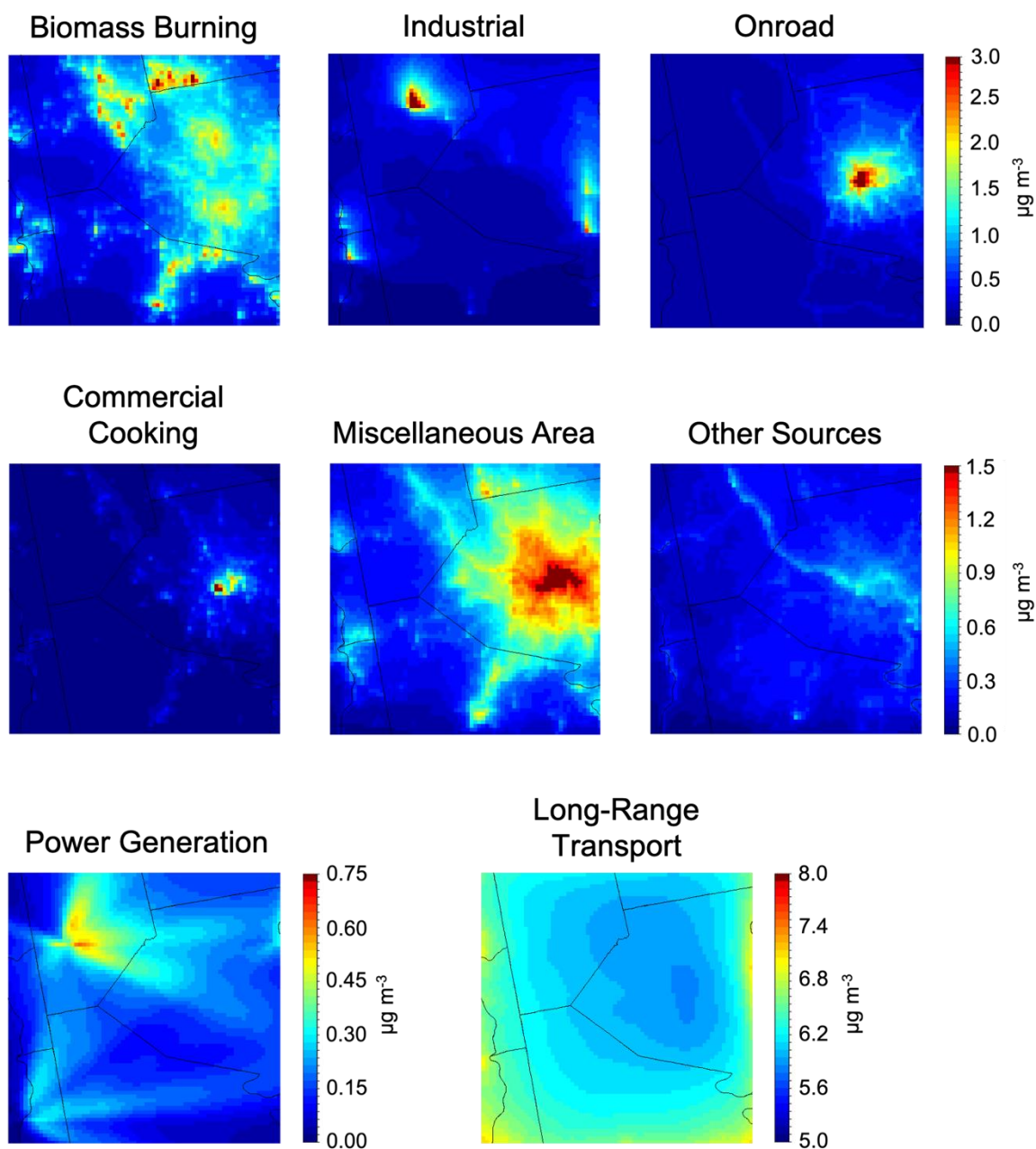


Figure 4. Average predicted ground-level concentration of PM_{2.5} sulfate, nitrate and ammonium at a 36 x 36, 12 x 12, 4 x 4 and 1 x 1 km resolution during February 2017. Different color scales that do not start from zero are used for the various maps.



787

788

789 **Figure 5.** Contribution of each source to total PM_{2.5} during February 2017. Different scales
 790 are used for the various maps.

791

792

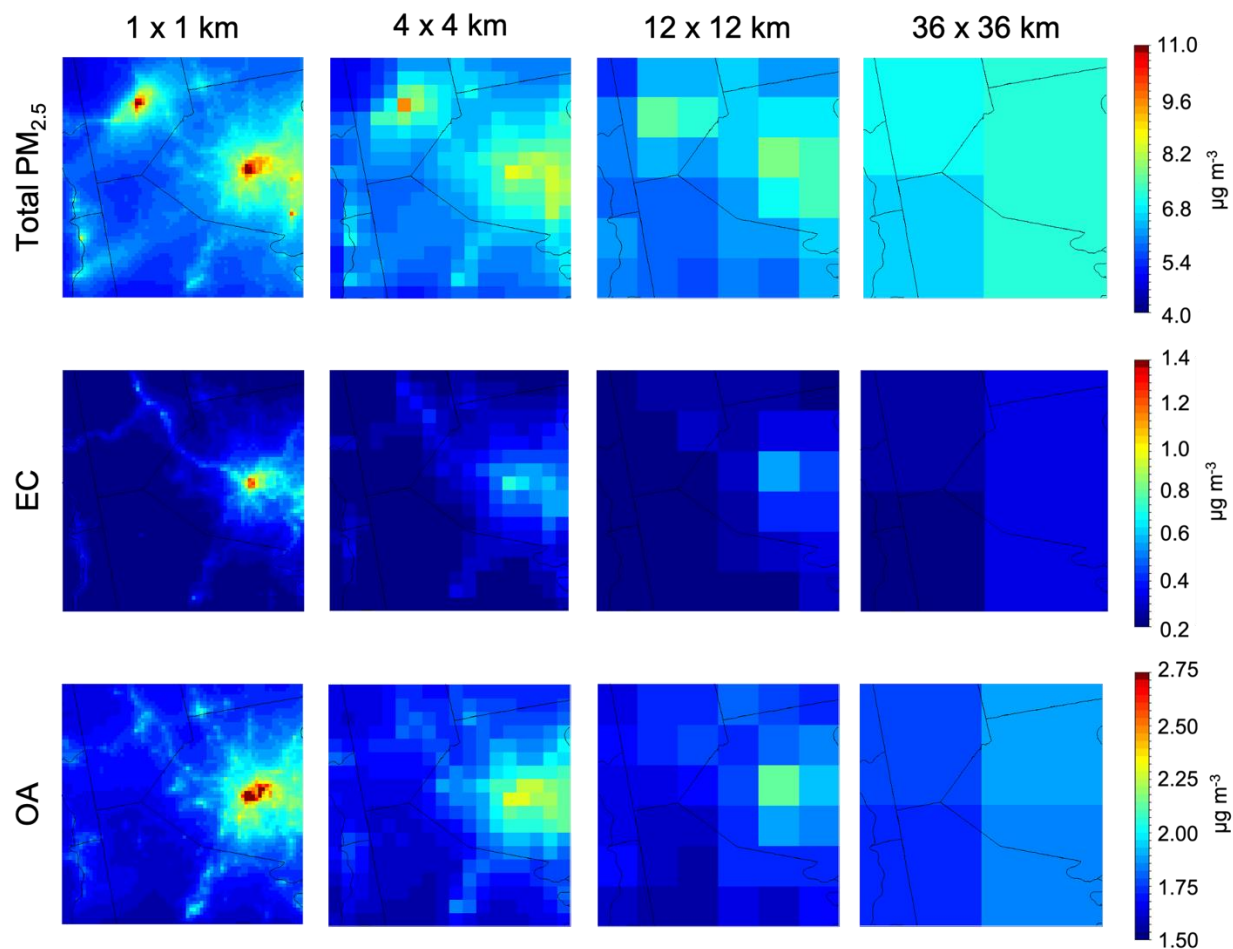


Figure 6. Average predicted concentration at the ground level of total $PM_{2.5}$, EC and OA at a 36x36, 12x12, 4x4 and 1x1 km during July 2017. Different color scales that do not start from zero are used for the various maps.

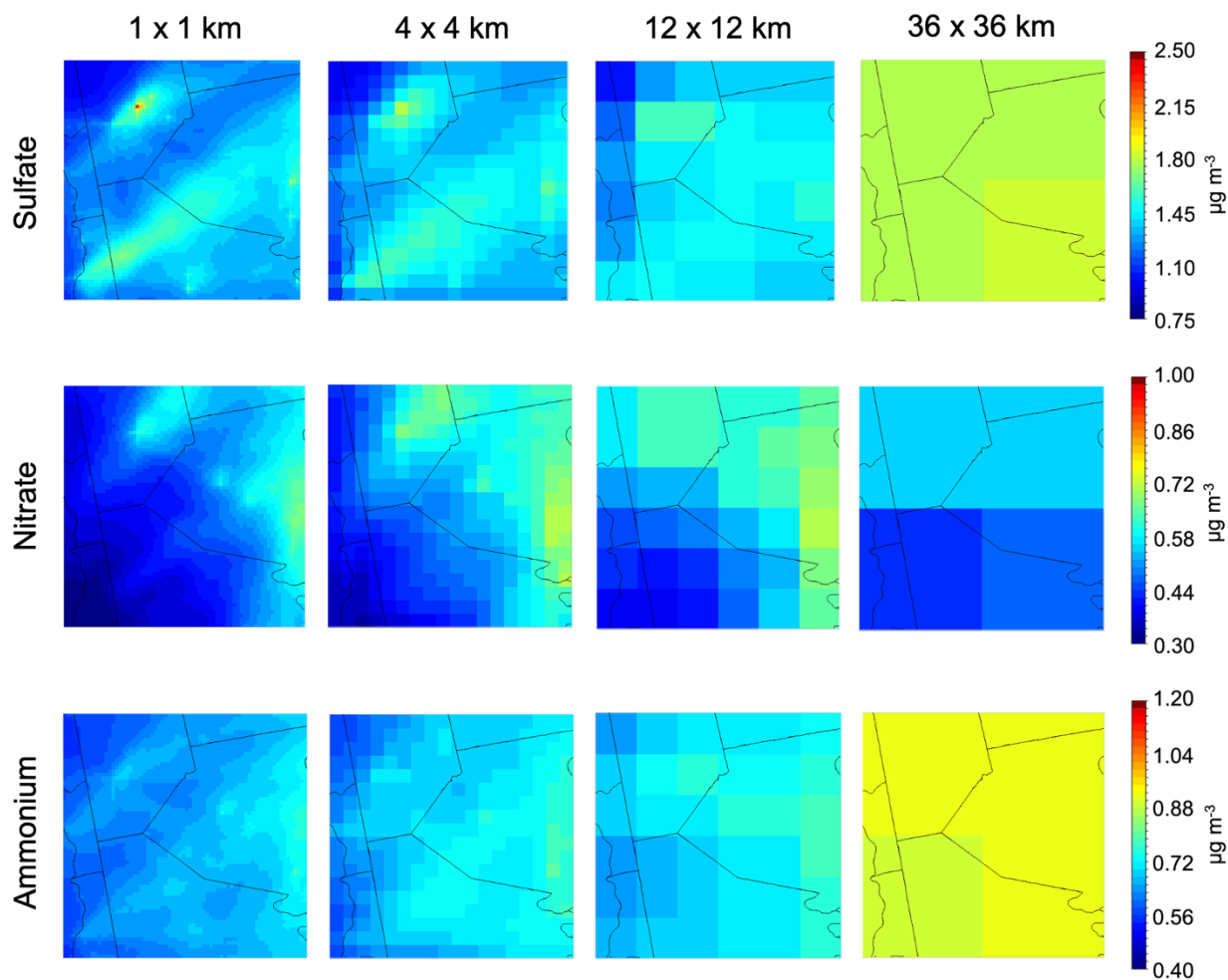
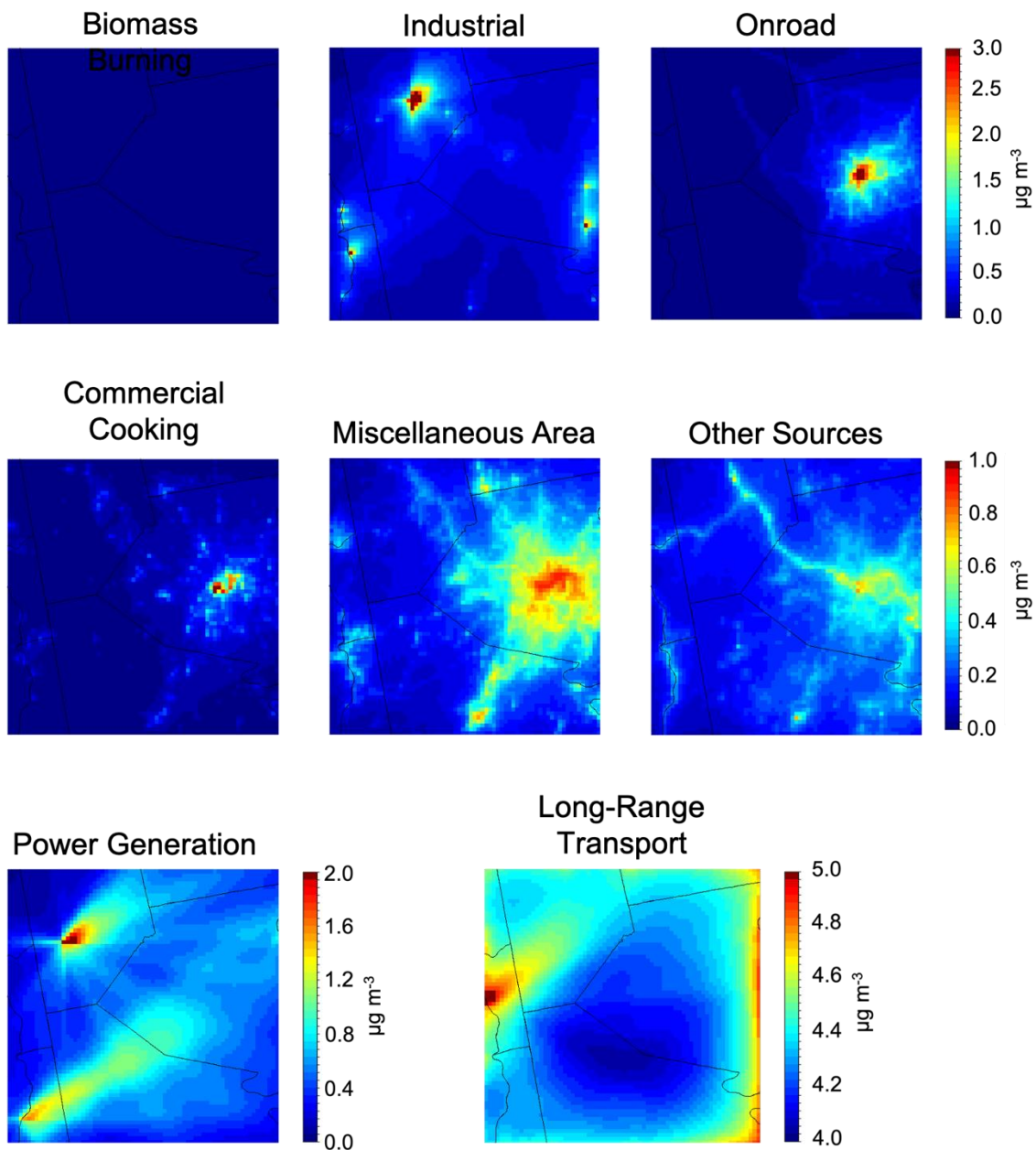


Figure 7. Average predicted concentration of PM_{2.5} sulfate, nitrate, and ammonium at a 36x36, 12x 12, 4x4 and 1x1 km during July 2017. Different color scales that do not start from zero are used for the various maps.



806

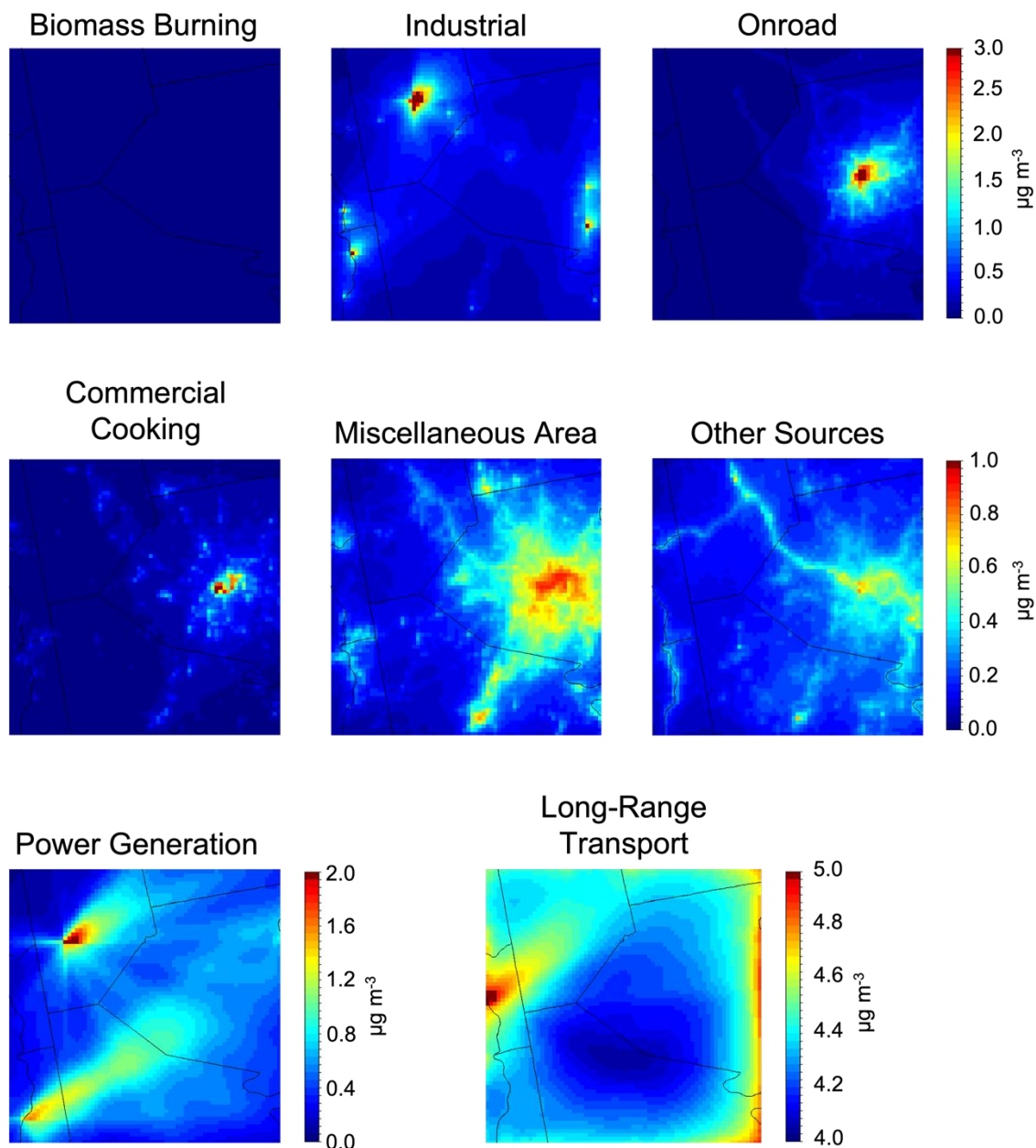


Figure 8. Contribution of each source to total $PM_{2.5}$ during July 2017. Different scales are used for the various maps.

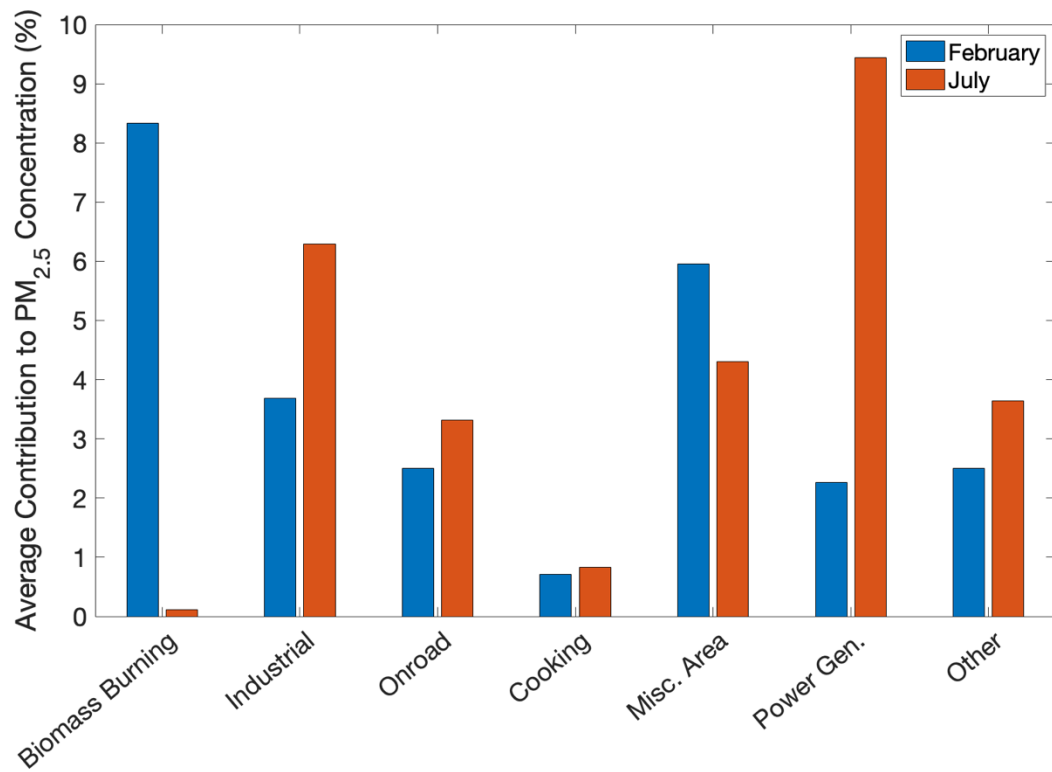


Figure 9. Relative contributions of local sources to average predicted total $PM_{2.5}$ concentrations in the [Allegheny County simulation inner 1x1 km resolution](#) domain during February and July 2017.

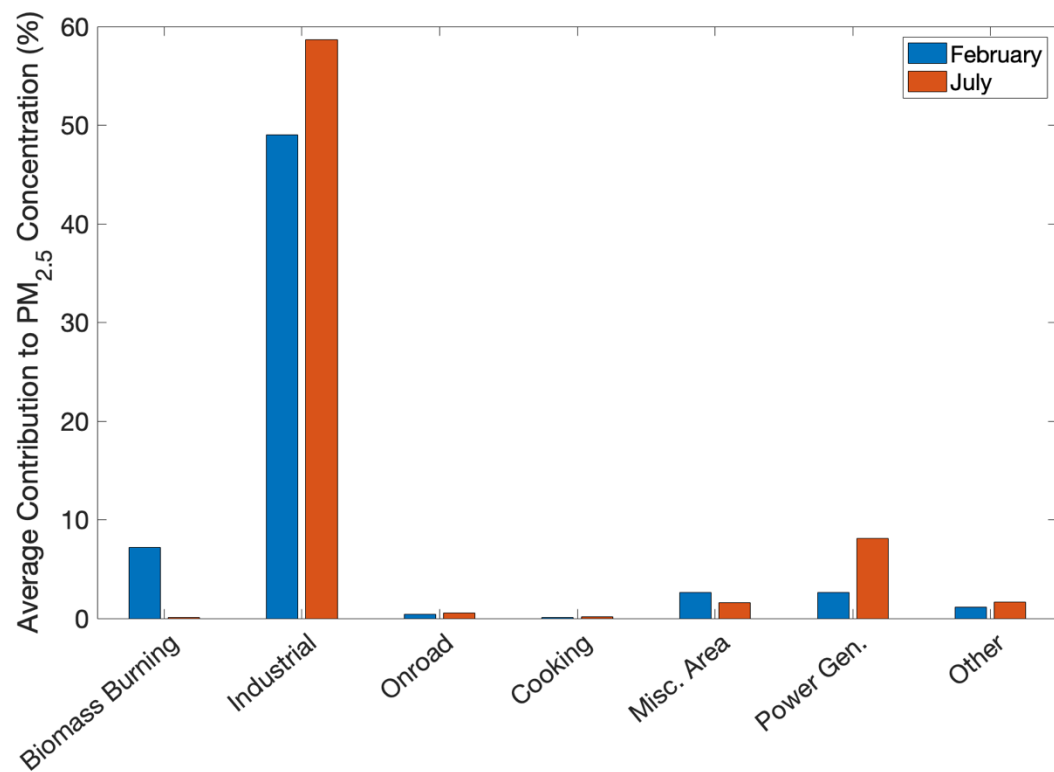


Figure 10. Relative contributions of local sources to average predicted PM_{2.5} concentrations at the location of highest average concentration (Beaver ~~Utter~~ County) during February and July 2017.

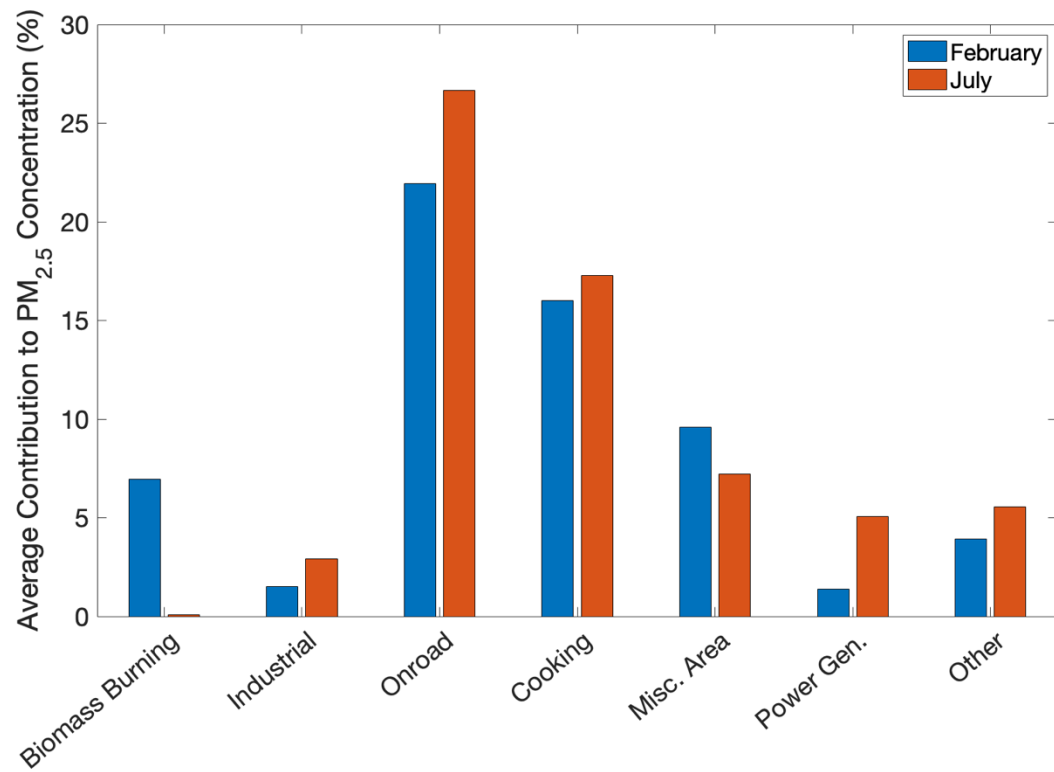
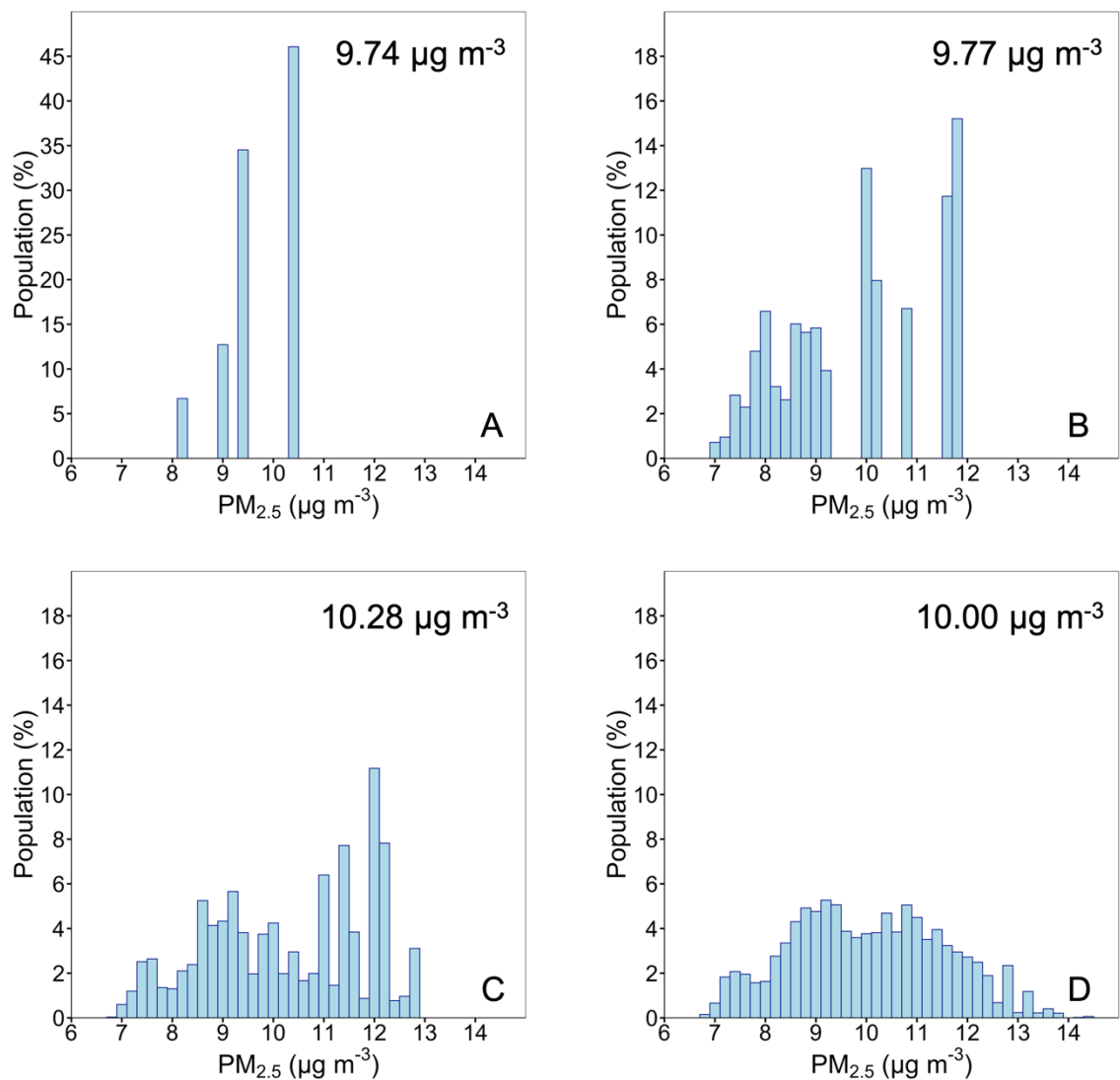


Figure 11. Relative contributions of local sources to average predicted total $PM_{2.5}$ concentrations in downtown Pittsburgh during February and July 2017.

827



828

829

830 **Figure 12.** Population exposure histograms at (A) 36x36, (B) 12x 12, (C) 4x4 and (D) 1x1
831 km during February 2017. A different scale for population is used for the distribution at 36
832 x 36 km resolution. The average population weighted $PM_{2.5}$ concentration for each
833 resolution is shown in the upper right corner of each window.

834

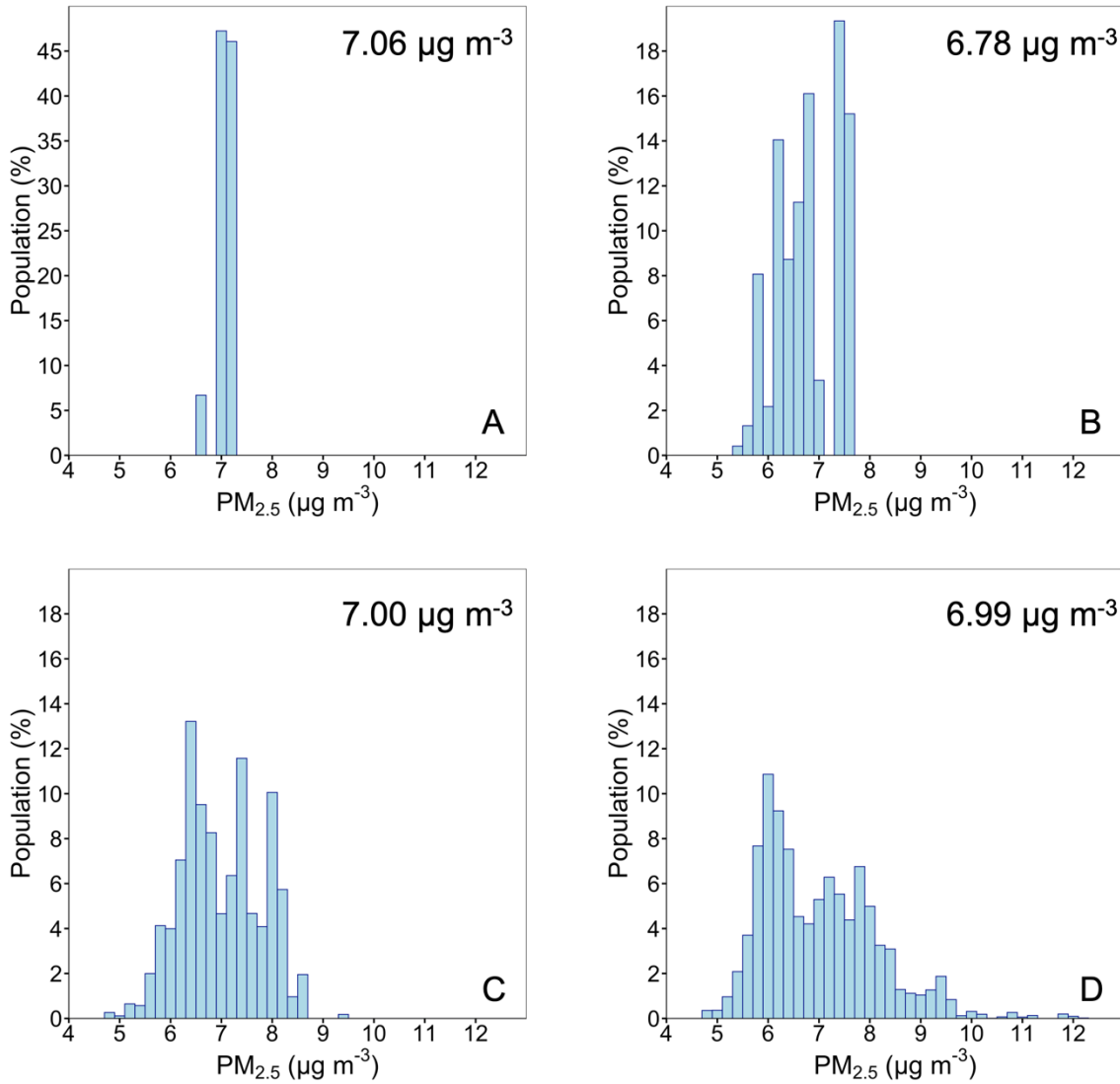
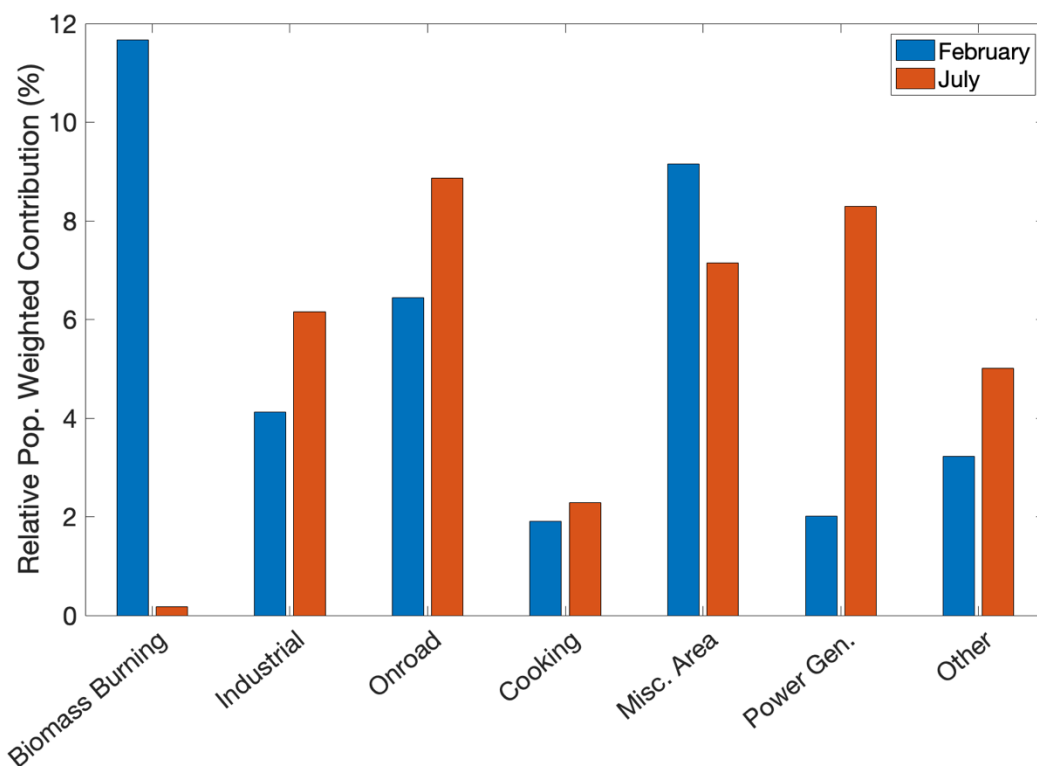


Figure 13. Population exposure histograms at (A) 36x36, (B) 12x 12, (C) 4x4 and (D) 1x1 km during July 2017. A different scale for population is used for the distribution at 36 x 36 km resolution. The average population weighted $PM_{2.5}$ concentration for each resolution is shown in the upper right corner of each window.

842

843



844

845 **Figure 14.** Relative contributions from local sources to population weighted total PM_{2.5}

846 concentration for February and July 2017.

847